BLOCKING THE ACQUISITION OF THE ESSENTIAL IRON NUTRIENT IN *PSEUDOMONAS AERUGINOSA*

By

MAMIE KANNON

Bachelor of Science in Microbiology, Cell and Molecular Biology

Oklahoma State University

Stillwater, OK

2020

Submitted to the Faculty of the

Graduate College of the

Oklahoma State University

in partial fulfillment of

the requirements for

the Degree of

MASTER OF SCIENCE

May, 2023

BLOCKING THE ACQUISITION OF THE

ESSENTIAL IRON NUTRIENT IN *PSEUDOMONAS*

AERUGINOSA

Thesis Approved:

Avishek Mitra, Ph.D.

Thesis Adviser

Erika Lutter, Ph.D.

Matthew Cabeen, Ph.D.

ACKNOWLEDGEMENTS

I would like to acknowledge my advisor Dr. Avishek Mitra for all the support and assistance throughout these last couple of years. Your teachings have helped me become a better student as well as microbiologist. To my committee members thank you for all your support and assistance as well. I am grateful to all of you.

I would also like to acknowledge my parents for their unwavering support, guidance, and faith in me. My sister Amelia for being the best sister a girl could ask for. To my fiancé Jeff, thank you for being there for me throughout this short but what felt incredibly long journey over the last two years. To my best friend Brooke, thank you for being there and supporting me no matter what. A huge thank you to all of you for your patience and support allowing me to complete my degree.

Name: MAMIE KANNON

Date of Degree: MAY, 2023

Title of Study: **BLOCKING THE ACQUISITION OF THE ESSENTIAL IRON NUTRIENT IN *PSEUDOMONAS AERUGINOSA***

Major Field: MICROBIOLOGY, CELL AND MOLECULAR BIOLOGY

Abstract: The Gram-negative opportunistic pathogen *Pseudomonas aeruginosa (Pa),* declared by the World health organization as a “Priority 1: Critical Pathogen," needs immediate new tactics for developing antipseudomonal treatments. *Pa* uses mechanisms to acquire ferric, heme (Hm), and ferrous iron from human hosts to survive, colonize and cause infection. Efforts have been made to create siderophore blockers to inhibit the ferric acquisition pathway of *Pa*. However, a lack of inhibitors exist to block the remaining Hm and ferrous pathways. We developed a targeted high throughput screening (HTS) approach and identified molecules that specifically inhibit the Hm and ferrous acquisition systems. We screened *Pa* against a small molecule library under three growth conditions. The iron source was the only variable, and each condition served as a counter screen for the other. We were able to identify econazole, bithionate, as growth inhibitors in Hm and oxyquinoline sulfate in ferrous iron. When exposed to meropenem, a commercial antipseudomonal, there was no interference in activity with some increased antipseudomonal activity. We examined each molecule's mechanisms of action to further understand interactions between *Pa* and the molecules. We also examined the effects of the compounds in the presence of biofilm and drug-resistant clinical isolates both in shaking and static conditions. The majority of the compounds showed specific activity in the respective iron sources against the isolates. Further analysis is needed to examine the mechanisms of action though initial experiments indicate that each compound has unique targets. In conclusion, we presented proof-of-concept of a successful targeted HTS, identified effective iron acquisition inhibitors against clinical isolates and started initial experiments to characterize the mechanisms of action of the newly identified inhibitors.

TABLE OF CONTENTS

Chapter Page
I. INTRODUCTION 1
1.1 Importance of Iron 1
1.2 Iron Acquisition in Bacteria 4
1.3 Iron Acquisition in Pseudomonas aeruginosa 7
1.4 Iron and Virulence in *Pa* 10
1.5 Iron Acquisition inhibitors- 14
1.6 General Aims 16
II. A NOVEL APPROACH TO IDENTIFY INHIBITORS OF IRON ACQUISITION SYSTEMS OF *PSEUDOMONAS AERUGINOSA.* 17
ABSTRACT 17
IMPORTANCE 18
INTRODUCTION 19
METHODS 21
Bacterial strains, growth media and molecules. 21
Iron-depletion of *P. aeruginosa* and determining growth conditions. 21
High throughput screening assay, compound library and identification of hit molecules. 22
Determining inhibition by hit molecules against *P. aeruginosa* through dose-response assays. 23
Statistical analysis. 23
RESULTS 24
Growth conditions for developing high throughput screening assay. 24
Determining robustness of the high throughput screening assay. 28
A targeted whole cell high throughput screening assay identifying inhibitors of heme and ferrous iron acquisition of *P. aeruginosa*. 30
Activity of heme- and ferrous-specific inhibitors. 33
Effect of HSI and FSI on meropenem activity. 35
DISCUSSION 37

Chapter Page

ACKNOWLEDGEMENTS 43

DATA AVAILABILITY 43

III. CHARACTERIZING FERROUS SPECIFIC AND HEME SPECIFIC INHIBITORS AND THEIR MECHANISMS OF ACTION 45

3.1 Background 45

3.2 Methods 47

Determining effect of inoculum on hit molecule activity. 47

Determine if HSIs bind heme iron or protoporphyrin (PPIX) ring. 47

Binding activity of HSIs and surprise hits using a Chrome Azurol S Assay (CAS) 48

Examining the effect of hit molecules against clinical *Pa* isolates. 49

3.3 Results 50

Effects of inoculum on hit molecule activity. 50

Heme, Protoporphyrin (PPIX), and HSI absorbance experiments 55

Determining iron chelating properties of hit molecules by CAS Assay. 64

Determining activity of hit molecules against *Pa* clinical isolates. 66

3.4 Discussion 73

IV. CONCLUSION 77

REFERENCES 81

LIST OF FIGURES

Figure Page

1.1. Importance of Iron- 3

1.2. Iron Acquisition in Bacteria- Iron acquisition in Gram-negative bacteria. 6

1.3. Iron Acquisition in *Pseudomonas aeruginosa*.....9

1.4. Iron and Virulence in *Pa*-....13

1.5. Iron acquisition inhibitors-....15

2.1. Iron depletion of *P. aeruginosa*. 26

2.2. Iron-specific growth conditions of *P. aeruginosa*. 27

2.3. High throughput screening (HTS) assay performance.....29

2.4. Specific activity of hit molecules determined by dose-response assays.....32

2.5. Effect of iron concentration on heme- and $FeSO_4$-specific inhibitors. 34

2.6. Effect of heme- and $FeSO_4$-specific inhibitors on activity of meropenem. 36

3.1. Effect of increased inoculum on Econazole activity 52

3.2. Effect of increased inoculum on Bithionate activity....53

3.3. Effect of increased inoculum on Oxyquinoline Sulfate activity 54

3.4. Initial heme and PPIX absorbance experiments-....58

3.5. Changes in absorbance of PPIX and heme in the presence of Econazole-....59

3.6. Changes in absorbance of PPIX and heme in the presence of Bithionate-....60

3.7. Changes in absorbance of heme and PPIX in the presence of Raloxifene-....61

3.8. Changes in absorbance of heme and PPIX in the presence of Tannic Acid- ..62

3.9. Changes in absorbance of heme and PPIX in the presence of Zinc Pyrithione- 63

3.10. Chrome Azurol S Assay- 65

3.11. Initial Growth of Clinical Isolates in LB 68

3.12. *5715d* Shaking and Static growth experiments- 69

3.13. *112014b* Shaking and Static growth experiments- 70

3.14. *3614b* Shaking and Static growth experiments- 71

Figure Page
3.15. *9414d* Shaking and Static growth experiments- 72

CHAPTER I

INTRODUCTION

1.1 Importance of Iron

Iron is an essential nutrient for most living organisms. The ability to cycle between ferric and ferrous oxidation states makes iron an essential cofactor for the activity of enzymes and molecules within most biological cells [1]. The average daily iron intake for humans is about 16-18 mg/day for men and 12 mg/day for women [2]. This small amount is essential for biological processes such as oxygen transport, immune function, DNA synthesis, and cellular respiration. In oxygen transport, iron is bound to hemoglobin within erythrocytes that carry oxygen to the lungs (Fig 1.1) [3]. The iron within hemoglobin can loosely bind oxygen, allowing oxygen transport through the bloodstream [3]. Iron also helps support the immune system by being a component of enzymes and proteins that assist in the growth and activity of immune cells such as, T cells, B cells, and macrophages (Fig 1.1) [4]. It is also necessary for the function of immune cells like cytokines which require iron for production [4]. Iron is crucial in energy production in the human body by facilitating the transport of electrons during cellular respiration. It is the component of many enzymes in the electron transport chain, the final step in cellular respiration. Electrons are passed to different enzymes creating a proton gradient to generate ATP [5].

Additionally, iron is a crucial component in molecules called cytochromes, heme-containing proteins. Cytochromes are used for shuttling electrons to various enzymes in the electron transport chain [6]. The synthesis of DNA would not be possible without iron as a

cofactor. Iron is a cofactor for ribonucleotide reductase, an enzyme that converts ribonucleotides to deoxyribonucleotides [7]. Many of these processes suffer if the human body is deficient in iron. Without adequate iron synthesis, specifically in oxygen transport, the human body can develop anemia, resulting in fatigue or shortness of breath. Iron deficiency in humans can also cause several other issues; irregular heartbeat, angina, heart attack, and a high childhood infection risk [8].

This balance of iron in the human body is essential to survival. Though iron is essential for vital processes in the human body, excess iron can also be toxic. This ability to transfer between redox cycles can form hydroxyl or lipid radicals, damaging proteins, DNA, and lipids in the host. Human host proteins like ferritin, transferrin, and lactoferrin combat this toxicity. Ferritin, a storage protein, binds excess iron in tissues like the liver, spleen, and bone marrow [2]. Transferrin, a transport protein, binds iron in the blood and transports it to cells throughout the body[2]. Finally, lactoferrin, a protein found in milk and other body fluids, binds iron, and transports it to various cells. Maintaining iron balance in the human body is essential to prevent toxicity and sustain many critical processes that allow survival.

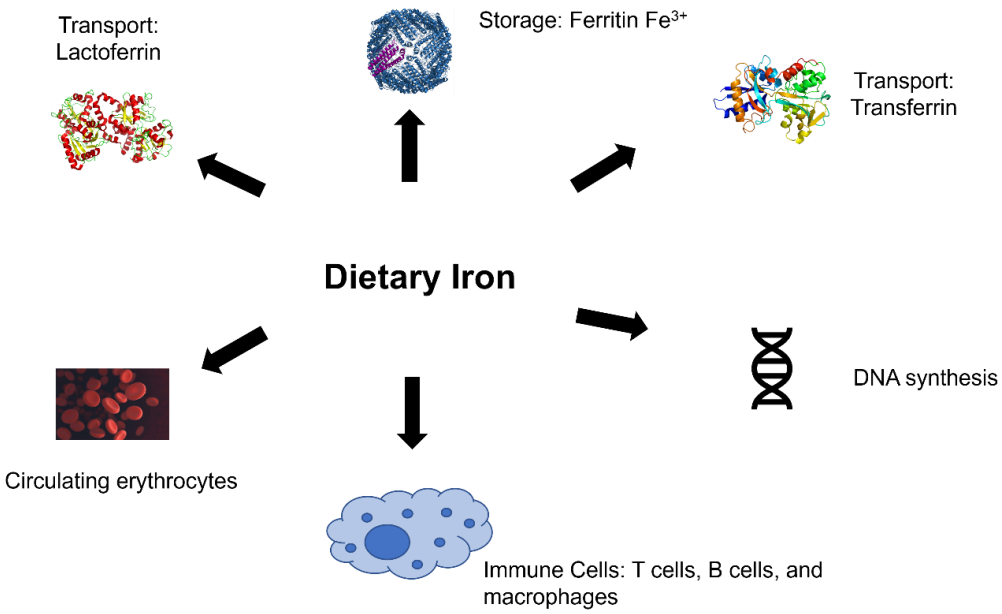

Figure 1.1. Importance of Iron-
The iron bound to circulating erythrocytes transport oxygen through the bloodstream. Iron helps support the immune system by being a component of enzymes and proteins that assist in the growth and activity of various immune cells. In addition, the synthesis of DNA would not be possible without iron as a cofactor. Iron is a cofactor for ribonucleotide reductase, an enzyme that converts ribonucleotides to deoxyribonucleotides.

1.2 Iron Acquisition in Bacteria

Iron is essential not only for human survival but also for the survival of bacteria. Like humans, bacteria also use iron for DNA replication, transcription, metabolism, and energy generation [9]. In addition, bacteria also use iron as a cofactor in many different proteins, such as cytochromes, tricarboxylic acid metalloenzymes, and respiratory proteins [10]. In order to survive in the human host and cause infection, bacteria have developed distinct mechanisms to acquire iron from the extracellular environment. Bacteria use various methods to acquire iron. In Gram-negative bacteria, iron is acquired in the ferric state, ferrous or through iron bound to a heme molecule (Fig 1.3 A). Expression of these pathways is controlled by ferric uptake regulator protein Fur [9]. Fur is a DNA binding repressor that uses ferrous iron as a cofactor; the protein binds to various iron-regulated genes at a "Fur box" to repress their expression at high iron concentrations [9]. When bound to ferrous iron, this repressor binds the Fur box blocking transcription of the iron uptake genes[11]. When iron is limited in the environment, the complex of Fur-Fe(II) disassociates from DNA and enables transcription of iron-regulated genes[9]. The ferric acquisition system of Gram-negative bacteria secretes iron-chelating molecules called siderophores. These siderophores have a high affinity for binding ferric iron. Secreted siderophores bind ferric iron; from various locations like, host iron-protein complexes, and deliver it to the bacterial cell surface by binding to an outer membrane receptor[12]. The ferric-siderophore complex is transported across the outer membrane into the periplasmic space and then transported into the cytoplasmic space by an inner membrane ABC transporter. From here, the iron is released by possible reduction of ferric iron to ferrous iron through reductase enzymes decreasing the stability of the siderophore complex [13]. After the siderophore is either degraded or recycled. [9]. The uptake process for heme iron has many similarities as discussed for siderophore-mediated iron acquisition. Heme is first sequestered from host hemoproteins by bacterial proteins called hemophores. Hemophores then deliver the

heme to an outer membrane receptor. These outer membrane receptors can also directly bind heme without the assistance of a hemophore. Heme is transported across the outer membrane into the periplasmic space and then transported into the cytoplasmic space by an inner membrane ABC transporter. In the cytoplasm heme can be degraded to release the iron stored within bacterial hemoproteins.

In ferrous iron acquisition system, ferrous iron is predicted to diffuse across the outer membrane through non-specific porin channels through non-specific porin channels. Once ferrous iron enters the periplasm it is transported by the inner membrane FeoABC transporter system, it is transported by the inner membrane FeoABC transporter into the cytoplasm [9]. FeoB is a primary transmembrane transporter acting as a permease, while FeoC regulates FeoB [9]. This is one of many ways bacteria obtain ferrous iron. For instance, some bacteria are capable of reducing ferric iron in order to solubilize for uptake [14].

Gram-positive bacteria also produce siderophores and hemophores for ferric and heme iron acquisition, respectively. The major difference in iron acquisition systems of Gram-positive results from the absence of an outer membrane. Gram-positive bacteria utilize cell surface attached lipoproteins for binding ferric-siderophores, heme-hemophores, host hemoproteins or free heme. The uptake of ferric-siderophores and heme across the cytoplasmic membrane very closely resembles that of Gram-negative bacteria as in transport by an ABC transporter (Fig 1.2). Ferrous iron acquisition in Gram-positives is the least investigated but is hypothesized to be imported directly by the FeoAB homolog transporter. Ferrous iron acquisition in Gram-positives is the least investigated but is hypothesized to be imported directly by the FeoAB homolog transporter [15].

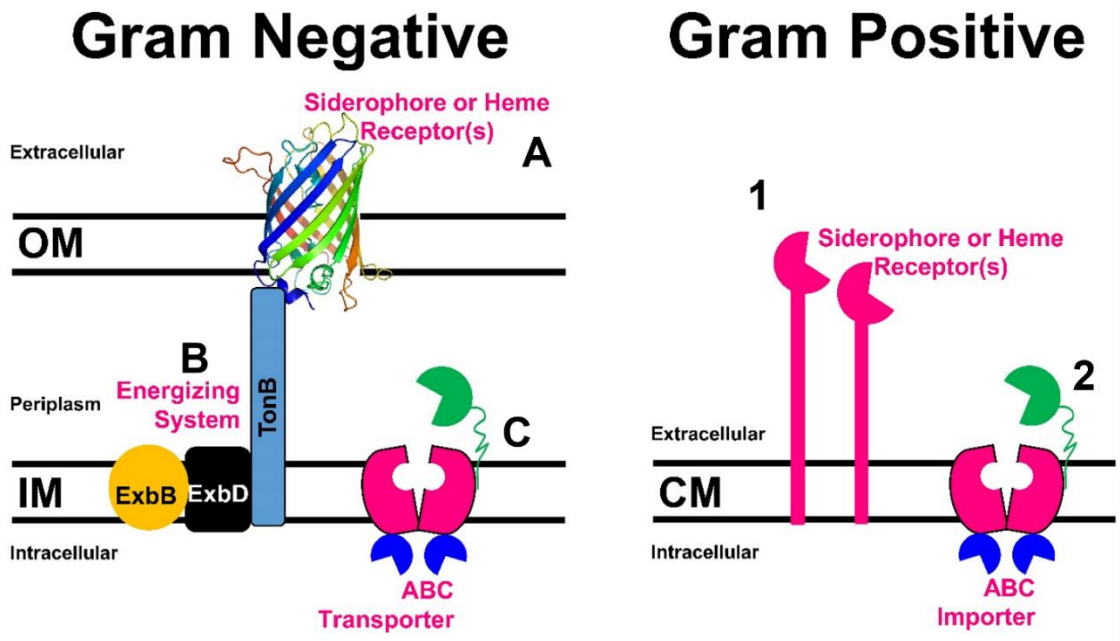

Figure 1.2. Iron Acquisition in Bacteria- Iron acquisition in Gram-negative bacteria. Siderophores with a high affinity for ferric iron are secreted into the extracellular space, binding to the ferric iron or heme, and delivering it to the cell by binding to the **siderophore or heme receptor (A.**). With the help of the TonB-ExbB-ExbD system (**B.**) the iron complex passes through the outer membrane into the periplasm. Next, the iron-siderophore complex passes to a periplasmic protein (green molecule), passing through an ABC transporter into the cytoplasmic space (**C.**). From here, the iron is released, and the siderophore is degraded or recycled.

Iron acquisition in Gram-positive bacteria. Gram-positive bacteria produce siderophores and hemophores for ferric and heme iron acquisition, respectively. Gram-positive bacteria do not have an outer membrane and instead use surface attached lipoproteins for binding ferric-siderophores (**1)**, heme-hemophore complex, host hemoproteins or free heme. The lipoproteins deliver the complex to an ABC importer **(2)**.

1.3 Iron Acquisition in Pseudomonas aeruginosa

Pseudomonas aeruginosa (Pa) is a Gram-negative opportunistic pathogen that uses three redundant mechanisms to acquire ferric, heme, and ferrous iron from the human host. These iron acquisition systems are vital for *Pa* to survive and colonize the human host, causing infection.

To acquire ferric iron, *Pa* uses two well characterized siderophores called pyochelin (PCH) and pyoverdine (PVD). PCH is typically secreted under normal growth conditions when iron is available and PVD is secreted under severely iron restricting growth conditions [16]. PVD is synthesized in the cytoplasm and then matures in the periplasm before being secreted through PvdRT-OmpQ an ATP- dependent efflux pump. When in the extracellular space, PVD chelates ferric iron by binding iron containing host proteins creating a Fe^{3+}-PVD complex which is bound by outer membrane channel proteins FpvAI and FpvB. Since transport of the Fe^{3+}-PVD complex across the outer membrane requires energy, the inner membrane TonB1-ExbBD system uses the proton motive force (PMF) to provide the energy for transporting the Fe^{3+}-PVD complex into the periplasm. The Fe^{3+}-PVD complex is bound by FpvC and FpvF in the periplasm and then transported into the cytoplasm by the inner membrane FpvDE ABC transporter [17, 18]. After the iron is released in the cytoplasm, PVD is recycled through the efflux pump PvdRT-OpmQ into the extracellular space to continue this cycle [17]. Similar to the PVD mechanism PCH chelates ferric iron and the Fe^{3+}-PCH complex is bound by the outer membrane receptor FptA. The complex is transported into the periplasm in a TonB1-dependent manner-and then transported into the cytoplasm by the inner membrane FptX transporter [19].

To acquire heme iron, *Pa* can utilize the Has or the Phu systems simultaneously. Heme uptake by the Phu and Has systems is mediated by the outer membrane receptors PhuR and HasR, respectively. The two systems differ in that PhuR binds free host heme directly, where HasR gets

heme delivered to it by the *Pa* hemophore protein HasA [20]. HasA first sequesters heme from host hemoproteins such as hemoglobin to deliver heme to HasR. Following heme binding by PhuR or HasR, heme is transported into the periplasm in a TonB-dependent manner, bound by periplasmic binding protein PhuT and then transported into the cytoplasm by the inner membrane ABC transporter PhuUV. Within the cytoplasm the chaperon protein PhuS binds heme and delivers it to the heme oxygenase HemO, which cleaves the porphyrin ring to release the iron producing biliverdin, and carbon monoxide, as byproducts [20, 21].

Unlike the ferric form, ferrous iron is soluble and present in anaerobic or microaerobic conditions at low pH. The outer membrane receptor or channel required for ferrous iron uptake is unknown and hypothesized to be mediated by a non-specific porin. However, ferrous iron uptake across the inner membrane requires the FeoABC transporter [20]. This system is most often used when *Pa* finds itself in an oxygen restrictive environment, such as the cystic fibrosis (CF) lung. *Pa* also secretes molecules called phenazines to reduce ferric iron to ferrous iron. This increases the solubility of iron and then allows the iron to be transported by the Feo system. Phenazine-1-carboxylic acid, the precursor of pyocyanin, and pyocyanin itself, a phenazine, can reduce ferric iron, that may be bound to host proteins, to the more soluble ferrous, allowing the Feo system to be used in these oxygen restrictive environments [20]. All three iron acquisition systems are essential to the survival of *Pa*. Each acquisition system is independent, allowing survival in many environments, such as oxygen-restrictive, heme-dominated, or iron restrictive [20].

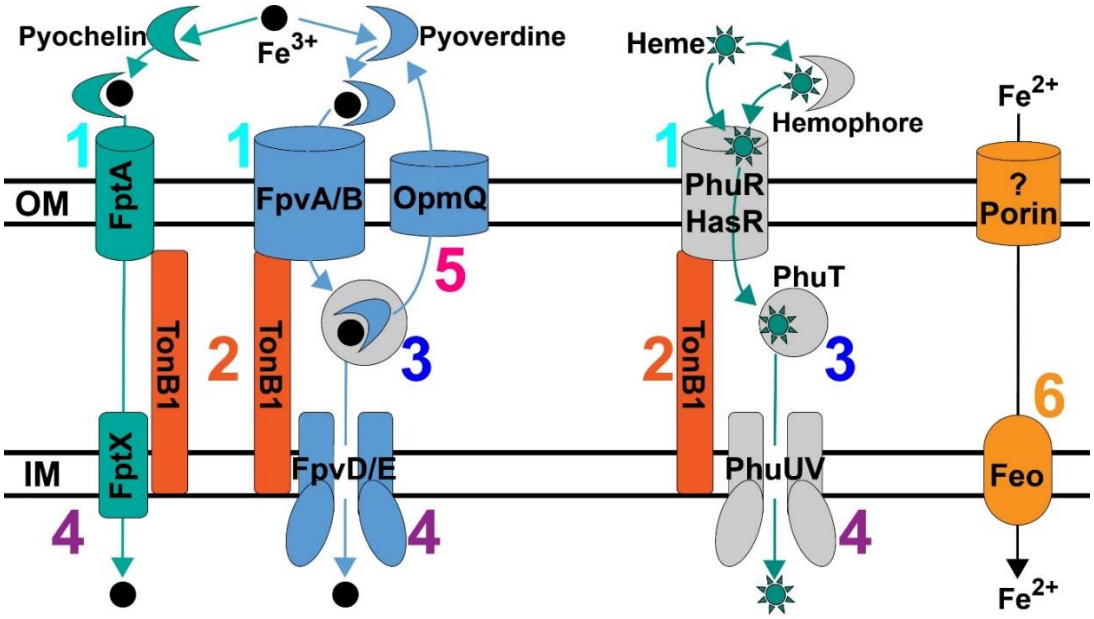

Figure 1.3. Iron Acquisition in *Pseudomonas aeruginosa*.
(1) Outer membrane receptor(s) bind pyochelin or pyoverdine*[22, 23]* or Hm or Hm-hemophore*[24, 25]*. **(2)** Uptake across the OM is completely dependent on the TonB1 system. **(3)** Substrate binding protein(s) bind ferric-siderophore*[26]* or Hm*[27]* in the periplasm. **(4)** Inner membrane (IM) permease transports ferric-iron**(3)** Substrate binding protein(s) bind ferric-siderophore*[26]* or Hm*[27]* in the periplasm. **(4)** Inner membrane (IM) permease transports ferric-iron*[18]* or Hm*[27]* into the cytoplasm. or Hm*[27]* into the cytoplasm. **(5)** Deferrated siderophores are recycled*[28]*. **(6)** Ferrous iron is hypothesized to diffuse through porin(s) and then transported by the IM FeoABC system*[14]*. **(7)** *Pa* can also utilize xenosiderophores*[20]* (siderophores from other bacteria), omitted here for simplicity. **(7)** *Pa* can also utilize xenosiderophores*[20]* (siderophores from other bacteria), omitted here for simplicity.

1.4 Iron and Virulence in *Pa*

Pa is a main cause of nosocomial infections as well as chronic infections in CF patients [29, 30]. *Pa* also has a high mortality rate for patients with CF[31]. Iron is vital for *Pa* virulence factors in many ways. All three iron acquisition pathways are vital for survival and infection. As shown in Minandri *et al.* iron uptake mutants with a *tonB1 and feoB* deletion did not grow aerobically under low iron conditions and was avirulent in a mouse model [32]. Pyoverdine, the siderophore used in ferric iron acquisition, also contributes to virulence in *Pa* [33]. Another finding in Minandri *et al.* described pyoverdine mutants (*pvdA)* and a siderophore mutant (*pvdApchD)* did not grow in human serum and caused low mortality in mice, however a double deletion mutant of *pvdAfpvR* restores the lethal phenotype[32]. This double deletion mutant expressed wild type levels of pyoverdine regulated virulence factors without the ability to produce pyoverdine showing pyoverdine contributes to pathogenesis with virulence inducing-capabilities combined with iron transport. In the CF lung mutants that are negative for pyoverdine actually accumulate in the CF lung while siderophore uptake genes are reduced in sputum [34-36]. Additionally ferrous iron is abundant in the CF lung at around 39 μM whereas ferric iron is not as abundant[37].

Pa uses the Fur system to regulate the expression of iron acquisition systems. In restrictive iron environments, Fur can regulate various expression of iron acquisition and virulence factors[38]. Studies done with exotoxin A, a dangerous A-B exotoxin in *Pa*, showed Fur regulating its expression [39]. The binding of PVD to the outer membrane FpvA elicits a signal cascade through an FpvR anti-sigma factor [38]. FpvR also controls two alternative sigma factors, PvdS and FpvI. PvdS promotes the expression of pyoverdine biosynthesis genes and exotoxin A while FpvI recruits RNA polymerase to the promoter gene for FpvA [38]. PvdS is known to directly bind to gene promoters of two upstream regulatory proteins that promote the expression of toxA, RegA,

and PtxR. However, it is unclear if PvdS affects expression by directly binding to the toxA promoter [38, 40, 41].

Biofilm formation significantly contributes to *Pa* virulence by assisting in antibiotic resistance. Ferrous iron regulation has been shown to play a part in this biofilm formation and antibiotic resistance. In *Pa,* the protein *feoB,* a putative G-protein-like permease, was shown to facilitate biofilm formation in the presence of phenazines while being directly regulated by the Fur protein [42, 43]. Iron in excess is needed for biofilm formation, and *Pa* phenazines' presence allows excess iron to be available to the bacteria [44, 45]. Furthermore, it has been shown that biofilm formation can proceed without *Pa* siderophores through the reduction of Fe(III) to the more favorable Fe(II) with the help of these phenazines [42]. Biofilm formation is hazardous for CF patients, where ferrous iron is more abundant [37]. This accumulation of biofilm in the CF lung allows for the persistence of antibiotic resistance, and the emergence of chronic *Pa* infection, making ferrous iron an essential part of *Pa* virulence.

Heme acquisition's contribution to virulence is less defined than that of the ferric and ferrous pathway. Once internalized in *Pa,* it may regulate gene expression through metabolic feedback. HemO degrades heme to biliverdin producing carbon monoxide and iron, but this biliverdin isomer pattern is unique to *Pa* [38]. This unique isomer pattern has been shown to allow positive feedback of production of the HasA hemophore and a decrease of production in isomer mutant strains compared to PAO1 wild-type strain (WT) [46]. Similar to the abundance of ferrous iron in the CF lung, there is an upregulation of heme and ferrous genes within the CF lung, allowing for the persistence of infection [36].

Iron is not only important to the survival of *Pa* but also crucial for the virulence factors that make *Pa* an opportunistic pathogen. With iron being essential for survival and supporting virulence factors, these pathways would be ideal targets for antipseudomonal treatment.

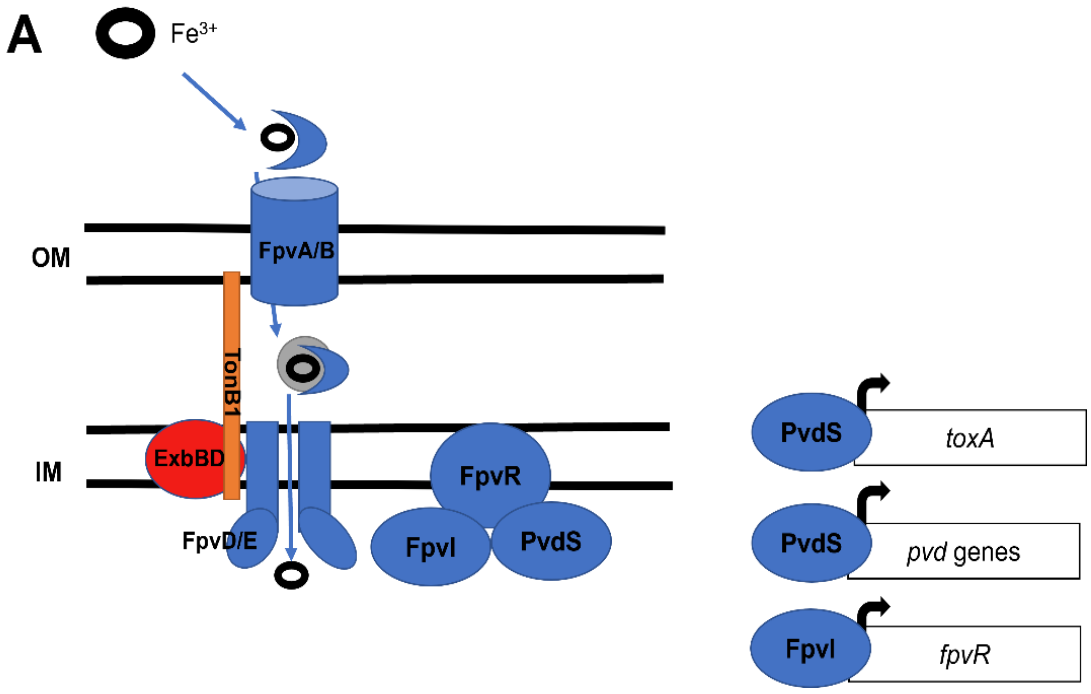

Figure 1.4. Iron and Virulence in *Pa-*
The binding of PVD to FpvA elicits a signaling cascade to FpvR that controls two alternative sigma factors, PvdS and FpvI. PvdS promotes the expression of pyoverdine biosynthesis genes and exotoxin A.

1.5 Iron Acquisition inhibitors-

Previous studies have identified iron acquisition inhibitors of *Pa*, specifically ferric iron acquisition inhibition, as an attempt to stop *Pa* metabolism. Gallium (III) structurally resembles ferric iron and is recognized by iron acquisition systems [47]. Gallium (III) may structurally resemble ferric iron and bind siderophores but lacks the redox activity of ferric iron. Depending on the siderophore, it is bound to affect the bacteria differently. For example, if Gallium (III) binds to pyochelin, it is still deposited in the cell but interferes with cell function[48]. Gallium (III) has been investigated *in vitro* and *in vivo* against *Pa* with CF patients because of *Pa's* high rate of infection and mortality due to this bacteria. Additionally, Kirienko *et al.* discovered anti-pyoverdine specific compounds that reduced the pathogenesis of *Pa* [49]. However, these ferric inhibitors only partially eliminate *Pa* infection due to *Pa's* ability to use the other two iron acquisition pathways. In addition to not eliminating the bacteria: *Pa* upregulates heme and ferrous genes in the CF lung, siderophore mutants accumulate in the CF lung, and ferrous iron is abundant in the CF lung [36, 37]. In order to eliminate *Pa* infection, all three iron acquisition systems need to be inhibited.

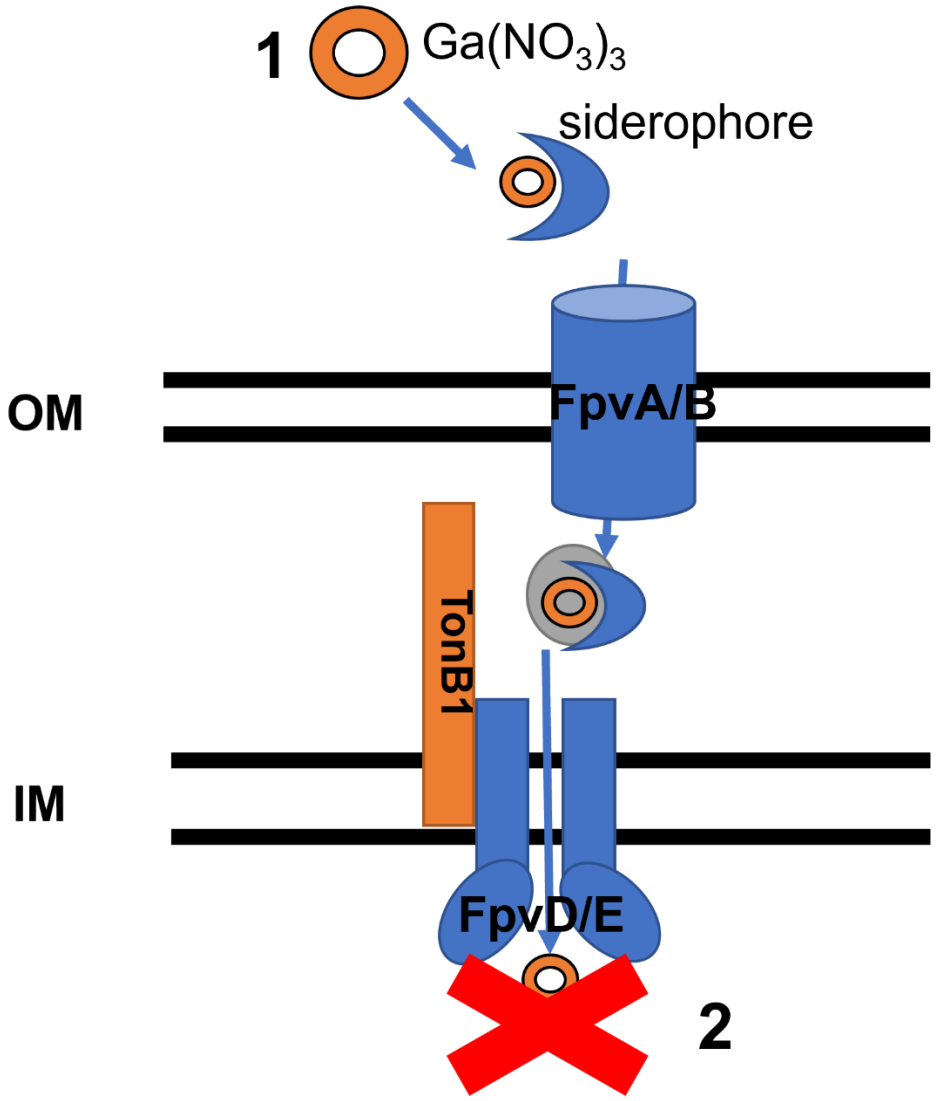

Figure 1.5. Iron acquisition inhibitors-
The binding of gallium nitrate to the siderophore pyoverdine is similar to ferric iron **(1)**. Once gallium nitrate passes through the periplasm and into the inner membrane because of the lack of redox activity it cannot be used in any essential processes (**2)**.

1.6 General Aims

Ferric iron acquisition inhibitors have been identified in *Pa*; however, they are ineffective in eliminating *Pa* due to *Pa's* two other ferrous and heme iron acquisition pathways. Using *Pa* as a model organism, this study strives to identify inhibitors of the ferrous and heme pathways using a HTS approach. According to the CDC, *Pa* alone is responsible for about 51,000 hospital infections, with about 13% being multidrug-resistant. This study's general hypothesis is that identifying ferrous and heme iron acquisition inhibitors can work synergistically with a ferric iron acquisition inhibitor, effectively starving *Pa* of an essential nutrient and killing the bacteria.

Below are the aims to test this hypothesis:

Aim 1. Using a HTS approach, identify molecules that inhibit the growth of *Pa* in the presence of ferrous or heme iron.

Aim 2. Determine the efficacy of inhibitors against drug-resistant strains of *Pa* and characterize the binding activity of each compound and their respective iron source.

CHAPTER II

A NOVEL APPROACH TO IDENTIFY INHIBITORS OF IRON ACQUISITION SYSTEMS OF *PSEUDOMONAS AERUGINOSA.*

Note to Reader

This chapter has been previously published in *Microbiology Spectrum*, 2022; 10(5): e02437-22, and has been reproduced as per open access guidelines of Microbiology Spectrum.

ABSTRACT

Pseudomonas aeruginosa (*Pa*) is an opportunistic pathogen which has been declared by the World Health Organization as a "Priority 1: Critical Pathogen" needing immediate new strategies for chemotherapy. During infection, *Pa* uses redundant mechanisms to acquire ferric, heme (Hm) or ferrous iron from the host to survive and colonize. Significant efforts have been taken to develop siderophore blockers to inhibit ferric iron acquisition by *Pa*, but there is a lack of inhibitors that can block Hm or ferrous iron acquisition by *Pa*. We developed and employed a targeted high throughput screen (HTS) and identified molecule(s) that can specifically inhibit Hm and ferrous iron acquisition systems of *Pa*. Our targeted approach relies on screening a small molecule library against *Pa* under three growth conditions, where the only variable was the iron source (ferric, Hm or ferrous iron). Each condition served as a counter screen for the other and we identified molecules that inhibit growth of *Pa* only in the presence of Hm or ferrous iron. Our data indicate that econazole, bithionate and raloxifene inhibit growth of *Pa* in the presence of Hm and oxyquinoline inhibits *Pa* growth in the presence of ferrous iron. These iron-specific inhibitors do not interfere with the activity of meropenem, a commercial antipseudomonal, and can also increase meropenem activity. In conclusion, we present proof-of-concept of a successful targeted

conditional screening method by which we can identify specific iron acquisition inhibitors. This approach is highly adaptable and can easily be extended to any other pathogen.

IMPORTANCE

Since acquiring iron is paramount to *P. aeruginosa* (*Pa*) survival and colonization in the human host, developing novel strategies to block access of *Pa* to host iron will allow us to starve it of an essential nutrient. *Pseudomonas aeruginosa* (*Pa*) uses siderophore, heme or ferrous iron uptake systems to acquire iron in the human host. We have identified a novel approach through which we can directly identify molecules that can prevent *Pa* from utilizing heme or ferrous iron. This approach overcomes the need for *in silico* designing of molecules and identifies structurally diverse biologically active inhibitor molecules. This screening approach is adaptable and can be extended to any pathogen. Since gram negative pathogens share many similarities in iron acquisition both at the mechanistic and molecular level, our screening approach presents a significant opportunity to develop novel broad spectrum iron acquisition inhibitors of gram-negative pathogens.

INTRODUCTION

Pseudomonas aeruginosa (*Pa*) is a ubiquitous Gram-negative opportunistic pathogen that resides in a wide range of environments [50]. It is the leading cause of nosocomial infections and ventilator-associated pneumonias in the US and is associated with extremely high mortality rates ranging from 13-50% [51-53]. *Pa* also causes chronic pulmonary infections in lungs of patients with cystic fibrosis (CF) and results in the death of 80% of CF patients [30, 31]. Recent CDC estimates show that yearly there are ~51,000 hospital-associated *Pa* infections with 13% of those infections being caused by multidrug resistant *Pa* (MDR-*Pa*). The long treatment times for MDR- and pan-drug resistant (PDR-) *Pa* increase the risk of selecting for new resistant strains and pose a large economic burden, with average patient treatment costs being as high as $67,000 [54]. Due to the numerous mechanisms of resistance of *Pa* to antibiotics, a serious roadblock to treatment has been the lack of drugs inhibiting growth or killing *Pa* by new molecular mechanisms. The combination of Ceftolozane/tazobactam (C/T) was the last FDA-approved treatment for drug-resistant *Pa* in 2014 and C/T-resistant *Pa* was identified the same year [55]. Resistance mechanisms to all known antibiotic agents have been identified in *Pa* leading the World Health Organization to declare *Pa* as a "Priority 1: Critical" pathogen needing new strategies and options for prevention and chemotherapy [56].

An attractive area of research to develop novel antipseudomonals has been to inhibit iron acquisition by *Pa*. Iron is an essential micronutrient for most living organisms and *Pa* is completely dependent on iron acquisition to successfully colonize the human host [20, 32, 36]. To restrict growth of any invading pathogens, the human host sequesters iron within heme (Hm) or in high-affinity binding proteins such as transferrin (Tf), lactoferrin (Lf) or ferritin [57, 58]. *Pa* overcomes iron limitation in the host by: i) secreting the siderophores, pyoverdine and pyochelin [20], to chelate iron from host Tf, Lf or ferritin, ii) secreting a hemophore to capture Hm iron from host

hemoproteins [20], or iii) scavenging ferrous iron [14]. Since, it is known that pyochelin [59] and pyoverdine [32, 33, 60-62] are required for efficient colonization by *Pa* in murine infection models, considerable efforts have been dedicated to identify molecules to inhibit siderophore-mediated iron acquisition of *Pa* [63]. However, in clinical trials these siderophore inhibitors are only partially effective at restricting *Pa* infections [63] because *Pa* still utilizes the Hm and ferrous uptake systems to acquire iron from the host. Notably, Hm is the largest [64] source of host iron and the CF lung contains large amounts of ferrous iron (39 μM) [37]. Moreover, studies have clearly shown that *Pa* siderophore mutants successfully colonize lungs of CF patients [34-36] and that *Pa* downregulates siderophore production and upregulates Hm and ferrous iron uptake genes in the CF lung [36, 37]. These observations collectively show that *Pa* uses redundant iron uptake pathways *in vivo*. Therefore, to make inhibition of iron acquisition a viable strategy of antipseudomonal chemotherapy, all three (siderophore, Hm and ferrous) mechanisms of iron acquisition must be inhibited simultaneously *in vivo*. The fact that inhibitors of *Pa* Hm and ferrous iron uptake pathways have not been developed represents a major gap in our ability to inhibit iron acquisition of *Pa* and the goal of our study was to address this gap in knowledge. In this study, we developed a conditional screening approach to identify inhibitors of *Pa* Hm or ferrous iron utilization systems. We present proof-of-concept that this conditional screening approach can be employed to identify molecules that can specifically inhibit Hm or ferrous iron utilization by *Pa*.

METHODS

Bacterial strains, growth media and molecules.

Wild-type *Pseudomonas aeruginosa* strain PAO1 (PAO1) was routinely first streaked on solid LB agar plates and grown static at 37°C for 24 h. Liquid cultures were then initiated from a single isolated colony in LB broth and grown shaking at 200 rpm at 37°C. For growth assays, PAO1 was first iron-depleted by growing in defined succinate MOPS medium (SMM) [65] containing no iron (SMM-N) and then inoculated into SMM-N containing specific iron sources. Iron-free SMM-N was prepared in 1 L of ultrapure Millipore water using the following reagents: 0.01 g EDTA, 0.6 g KH_2PO_4, 0.9 g K_2HPO_4, 1.0 g NH_4Cl, 0.2 g $MgSO_4.7H_2O$, 0.075 g $CaCl_2.6H_2O$, 2.2 g sodium succinate, 0.1 g yeast extract, 0.4 g glucose, 2.0 ml trace elements, 2.0 ml vitamin solution, 40 mM MOPS, pH 6.8. Trace elements solution was prepared in 1 L of millipore water using the following reagents: 0.005 g $ZnSO_4$ $7H_2O$, 0.003 g $MnCl_2,4H_2O$, 0.002 g H_3BO_3, 0.005 g $CoCl_2,6H_2O$, 0.001 g $CuCl_2,2H_2O$, 0.002 g $NiCl_2$ $6H_2O$, 0.003 g $Na_2MoO_4.2H_2O$. The vitamin solution was prepared in 1 L of millipore water using the following reagents: 80 mg biotin, 400 mg Thiamine-HCl. $2H_2O$, 400 mg nicotinic acid, 20 mg of vitamin B12. Reagents were always sterilized using a 0.2 µm filter and never autoclaved. Econazole (E09575G), bithionate (T086525G), raloxifene (R01091G), tannic acid (AA3641022) and zinc pyrithione (50-199-8689) were purchased through Fisher Scientific. Oxyquinoline sulfate (55100-100G-F) was purchased through Sigma.

Iron-depletion of *P. aeruginosa* and determining growth conditions.

An overnight liquid starter culture of PAO1 was initiated by inoculating a single colony into 5 ml of LB. From the starter culture, PAO1 was then inoculated into 10 ml of fresh LB at an OD_{600} of 0.05. PAO1 cells were harvested from mid-logarithmic phase (Fig. 2.1 A), washed twice with 10 ml of PBS, and then inoculated into 10 ml of SMM medium containing no iron (SMM-N) at an initial OD_{600} of 0.5. To deplete internal iron reserves, cells were allowed to grow in SMM-N until

there was no change in optical density (Fig. 1B). Iron-depleted PAO1 cells were harvested and washed twice with 10 ml of PBS. PAO1 cells were then inoculated in 96-well plates at an OD_{600} of 0.01 to a final volume of 200 µl into SMM containing varying concentrations (Fig. 2) of ferric chloride ($FeCl_3$) or ferrous sulfate ($FeSO_4$) or hemin as the sole iron source. For medium containing $FeSO_4$, ascorbate (a reducing agent) was added to a final concentration of 2 mM and plates were wrapped with parafilm to maintain $FeSO_4$ in its reduced form as done in previous studies [32]. All plates were incubated at 37°C with shaking and optical density was monitored using a BioTek Synergy plate reader at 1 h intervals.

High throughput screening assay, compound library and identification of hit molecules.

High throughput screening (HTS) was performed at Southern Research (SR). A collection of 20,479 compound samples from Enamine and Microsource (Pharmakon 1600 library) was screened at a concentration of 10 µg/mL, 20 µg/mL or 50 µM, and a DMSO concentration of 0.4%. Compounds and DMSO carrier were dispensed into 384-well plates in 5 µL volume using the Biomek FX liquid handler (Beckman Coulter). Cells containing 0.4% DMSO served as the cell control (Cell Ctrl) and cells containing 20 µg/mL Meropenem as the positive control (Pos Ctrl). PAO1 was first iron-depleted as mentioned above and then added to three identically dosed 384-well plates at an OD_{600} of 0.001 to a final volume of 35 µL in SMM containing either 5 µM $FeCl_3$ or 5 µM $FeSO_4$ or 5 µM hemin, where the only variable between the three plates was the iron source. Plates were incubated at 37°C in a humidified atmosphere and OD_{600} was determined at 10 h using a CLARIOstar plate reader (BMG Labtech). Percent Inhibition was calculated as 100 x (Compound OD_{600} value – Median Cell control)/(Median Positive (Meropenem) control – Median Cell control)). The single concentration hit data was then analyzed to select molecules for dose response assays at Oklahoma State University. Molecules that inhibited growth of PAO1 by at

least 50% under only hemin or $FeSO_4$ growth conditions and were inactive in $FeCl_3$ condition were analyzed in dose response assays.

Determining inhibition by hit molecules against *P. aeruginosa* through dose-response assays.

PAO1 was first grown and then iron-depleted as mentioned above. In 96-well plates, washed PAO1 cells were inoculated at an OD_{600} of 0.001 to final volume of 200 µl into SMM containing 5 µM $FeCl_3$ or 5 µM $FeSO_4$ or 5 µM hemin as the sole iron source and increasing concentrations of hit molecules. All plates were incubated at 37°C with shaking and optical density was determined at 10 h using a BioTek Synergy plate reader.

Statistical analysis.

Sigmaplot (Systat Software) was used for statistical analysis. Where applicable statistical significance was determined by Tukey's Honest Significant Difference (HSD) test following an *F*-test. P values less than 0.05 are considered significant. All data presented are mean values with error bars representing standard error of mean values of at least three biological replicates.

RESULTS

Growth conditions for developing high throughput screening assay.

A main goal of this study was to identify inhibitors of Hm and ferrous iron acquisition of *Pa*. To achieve this goal, we developed a targeted whole cell high throughput screening (HTS) assay. In this HTS approach a compound library is simultaneously screened for antipseudomonal activity under three separate growth conditions, where the only variable is the iron source [ferric chloride ($FeCl_3$) or hemin (Hm) or ferrous sulfate ($FeSO_4$)] in the growth medium. Before inoculating *Pa* into the HTS screening medium, we had to ensure that all cellular iron reserves in *Pa* were depleted so that *Pa* strictly utilizes the iron source supplied in the screening medium. To this end, *P. aeruginosa* strain PAO1 was first grown in LB for 4 h to mid-exponential phase (Fig. 2.1 A) and cells from this phase were then inoculated at a high cell density in defined succinate MOPS medium containing no iron source (SMM-N). After 3 h of growth in SMM-N all internal iron reserves of *Pa* had been depleted as there was no change in optical density (Fig. 2.1 B). This regimen of iron-depletion was strictly followed before performing all growth experiments.

To develop the HTS assay, we first determined the growth conditions for the HTS screening medium. These growth conditions needed to establish two parameters: i) the concentration of $FeCl_3$, Hm or $FeSO_4$ to use in the screening medium where growth kinetics of *Pa* is comparable in all three conditions, and ii) the readout time when *Pa* reaches maximum growth in all three growth conditions. Knowing these conditions would allow us to appropriately identify molecules that inhibit growth of *Pa*. The screening medium for the HTS assay was prepared by adding $FeCl_3$, Hm or $FeSO_4$ to the base medium (SMM-N). We opted to not use artificial sputum medium (ASM) [66-73] for the screen, which is typically used in *Pa* and CF research. Instead, we utilized the chemically defined (SMM-N) medium because this allows us to manipulate the iron source and concentration, which is not possible in ASM. Ascorbate (a reducing agent) was added

to the $FeSO_4$ medium and plates were wrapped with parafilm to maintain $FeSO_4$ in its reduced form as done in previous studies for $FeSO_4$ growth experiments [32]. To determine the optimal HTS assay conditions, in 96-well plates iron-depleted *Pa* was inoculated into SMM-N containing varying concentrations of the $FeCl_3$, Hm or $FeSO_4$ and growth was recorded by monitoring OD_{600} (Fig. 2.2). Since it is impossible to remove all traces of iron from the medium, iron-depleted *Pa* cells were also inoculated in just SMM-N to determine the background growth from residual iron in the base medium. Compared to the background growth, we observed that *Pa* reached maximal growth at 10 h regardless of the iron source or concentration (Fig. 2.2 all panels), which also demonstrated that ascorbate does not influence the growth kinetics of *Pa*. However, *Pa* achieved similar maximal growth at 10 h with all iron sources at a final concentration of 5 µM (Fig. 2.2 C). Based on these observations we determined that in the HTS assay the optimal concentration for all iron sources is 5 µM and the optimal time for readout is at 10 h.

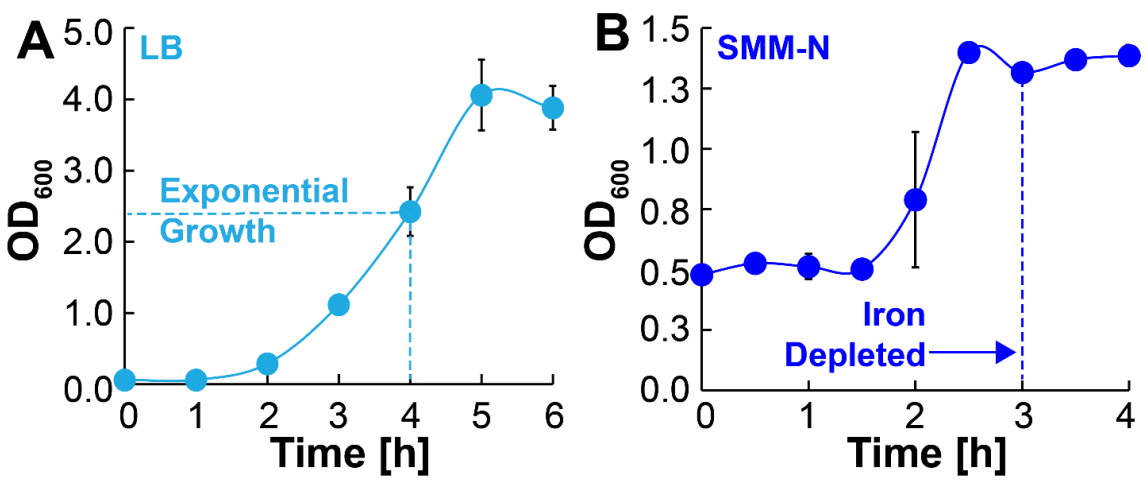

Figure 2.1. Iron depletion of *P. aeruginosa*.
A. Growth of wild-type *P. aeruginosa* PAO1 in LB to determine exponential and stationary growth phase of PAO1. **B.** To deplete internal iron reserves of PAO1, mid-log LB phase cells were inoculated in succinate MOPS medium (SMM) containing no iron (SMM-N) and allowed to grow until there was no change in optical density. Error bars represent standard error of mean (SEM) of three biological replicates. In many cases error bars are smaller than marker data points. Source data file is provided.

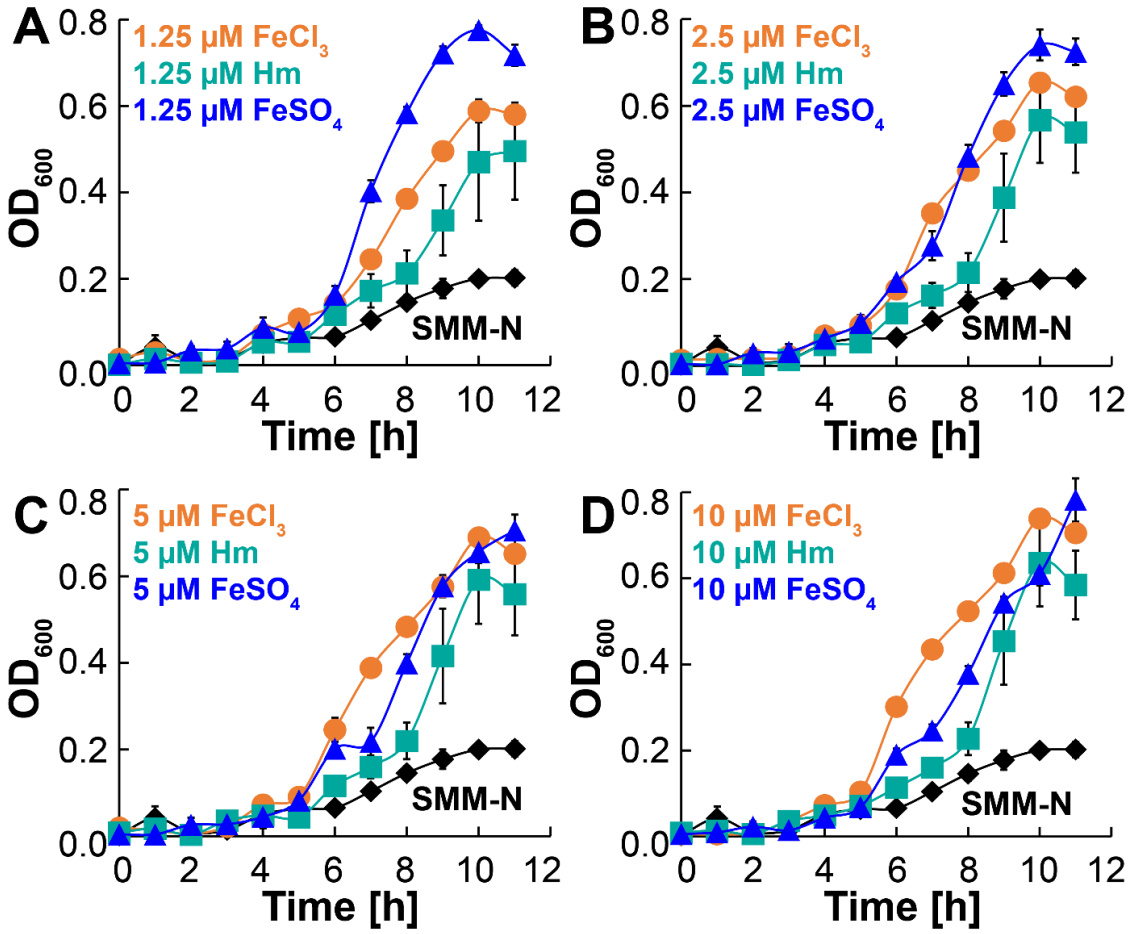

Figure 2.2. Iron-specific growth conditions of *P. aeruginosa*.
Growth of iron-depleted PAO1 cells in SMM-N containing ferric chloride ($FeCl_3$ – orange circles) or hemin (Hm – cyan squares) or ferrous sulfate ($FeSO_4$ – blue triangles) at a final concentration of either 1.25 µM **(A)** or 2.5 µM **(B)** or 5 µM **(C)** or 10 µM **(D)**. Iron-depleted PAO1 was also grown in just SMM-N (black diamonds) to determine background growth from any residual iron in the medium. Note: For all panels data points for growth in SMM-N are the same. Error bars represent SEM of three biological replicates. In many cases error bars are smaller than marker data points. Source data file is provided.

Determining robustness of the high throughput screening assay.

As stated, our HTS approach involves screening a compound library simultaneously for antipseudomonal activity in three different iron sources (Fig. 2.3 A). To verify the robustness of our assay conditions, we determined the maximum and minimum growth of *Pa* in 384-well HTS plates. *Pa* was inoculated in SMM-N containing 5 µM $FeCl_3$ or Hm or $FeSO_4$ and grown for 10 h to determine maximum growth. Since PAO1 is susceptible to meropenem under all growth conditions (Fig. 2.3 B), we used 20 µM meropenem as a positive control for growth inhibition to determine minimum growth. We used optical density (OD_{600}) as a quantitative readout because it is inexpensive, requires few handling steps and is less prone to manipulation induced variations. Based on the maximum and minimum growth, we observed a strong signal to background (SB) ratio of >9 for all growth conditions (Fig. 2.3 C). The quality and performance of our HTS assay was determined by calculating the Z'-factor, which must ideally be in the range of 0.5-1.0 to be considered robust enough for HTS [74]. For all growth conditions, the Z'-factor in the 384-well format was >0.8 (Fig. 2.3 D), demonstrating that our assay is highly reliable and reproducible.

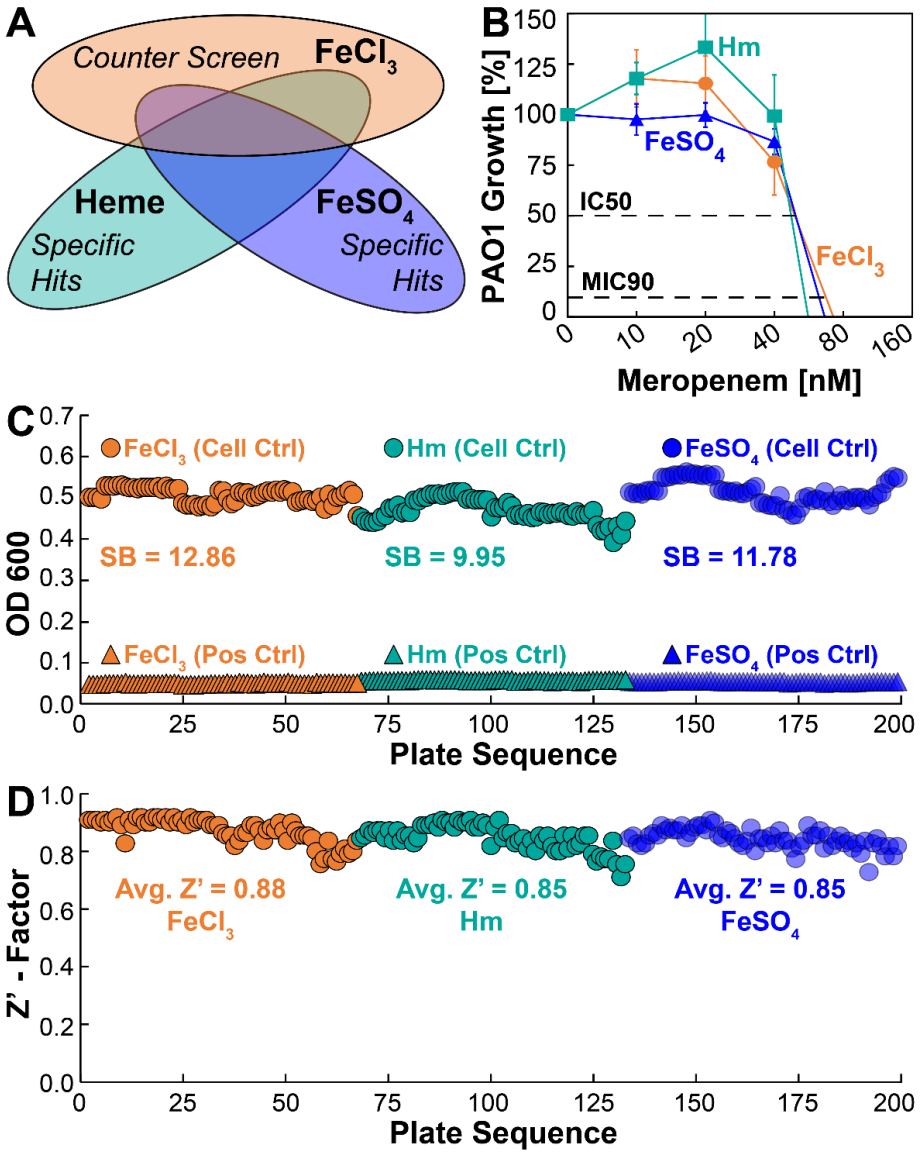

Figure 2.3. High throughput screening (HTS) assay performance.
A. Schematic representation of the three growth conditions used for high throughput screening of molecules. **B.** Survival of PAO1 in SMM-N containing 5 µM $FeCl_3$ (orange circles) or 5 µM Hm (cyan squares) or 5 µM $FeSO_4$ (blue triangles) in the presence of increasing concentrations of meropenem. PAO1 growth was monitored by measuring endpoint OD_{600} at 10 h and growth % was determined relative to growth of PAO1 in the absence of meropenem. Error bars represent SEM of five biological replicates. **C.** In 384-well plates, iron-depleted PAO1 was grown for 10 h in SMM containing 5 µM $FeCl_3$ or 5 µM Hm or 5 µM $FeSO_4$ in the absence (circles – cell control) or presence of meropenem (triangles – positive control). Control samples were arranged in 384-well plates in opposed quadrants. SB: signal to background ratio. **D.** Z'-factor was calculated for all plates and average (Avg.) Z-factor was determined for all three growth conditions. Source data file is provided.

A targeted whole cell high throughput screening assay identifying inhibitors of heme and ferrous iron acquisition of *P. aeruginosa*.

We performed a small proof-of-concept screen using a library of structurally diverse small molecules that serve as a basis for new lead discovery in HTS and to identify new activities in established drugs. Our goal was to demonstrate that our targeted whole cell screening approach can identify molecules that inhibit Hm and ferrous iron acquisition systems of *Pa*. The small molecule library was simultaneously screened against *Pa* in the three growth conditions where the $FeCl_3$ growth condition serves as a counter screen (Fig. 2.3 A). In principle, each screen serves as a counter screen for the others. Molecules that exhibit antipseudomonal activity only in the presence of Hm or $FeSO_4$ are considered as Hm-specific inhibitor (HSI) or ferrous-specific inhibitor (FSI), respectively (Fig. 2.3 A). Using this counter screening process of elimination, we identified three HSIs, one FSI and two molecules that inhibits growth of *Pa* in both $FeCl_3$ and Hm, which is a hit rate of ~0.3%.

We determined that econazole (Fig. 2.4 A), bithionate (Fig. 2.4 B) and raloxifene (Fig. 2.4 C) specifically inhibit growth of *Pa* only in the presence of Hm as the sole iron source but does not exhibit any activity against *Pa* in the presence of either $FeCl_3$ or $FeSO_4$. Dose response curves indicated an IC50 of ~10 µM for econazole and 6.3 µM for bithionate and raloxifene and MIC90 of ~20 µM and 12.5 µM for econazole and bithionate, respectively. While MIC90 for raloxifene in Hm was only achieved at a very high concentration of ~100 µM, it was still inactive in the presence of $FeCl_3$ and $FeSO_4$. We also determined that oxyquinoline sulfate (Fig. 2.4 D) specifically inhibits growth of *Pa* only in the presence of $FeSO_4$ as the sole iron source but does not exhibit any activity against *Pa* in the presence of either $FeCl_3$ or Hm. Dose response curves indicated an IC50 of ~11 µM and MIC90 of <20 µM for oxyquinoline sulfate. Surprisingly, we also identified two molecules that inhibit growth of *Pa* both in the presence of $FeCl_3$ and Hm.

Tannic acid inhibits growth of *Pa* in $FeCl_3$ and Hm with an IC50 ~1 µM and MIC90 of <10 µM (Fig. 2.4 E). However, tannic acid also exhibits some antipseudomonal activity in the presence $FeSO_4$ albeit to a much lower extent suggesting that it can also exert inhibitory activity against *Pa* growth in an iron-independent manner. Zinc pyrithione exhibits very similar antipseudomonal activity in both $FeCl_3$ and Hm with an IC50 ~10 µM and MIC90 of <12 µM (Fig. 2.4 F). Unlike tannic acid, zinc pyrithione does not exhibit any activity against *Pa* in the presence of $FeSO_4$. Altogether, these results demonstrate that our targeted whole cell screening approach successfully identified molecules that inhibit specific iron acquisition mechanisms of *Pseudomonas aeruginosa*.

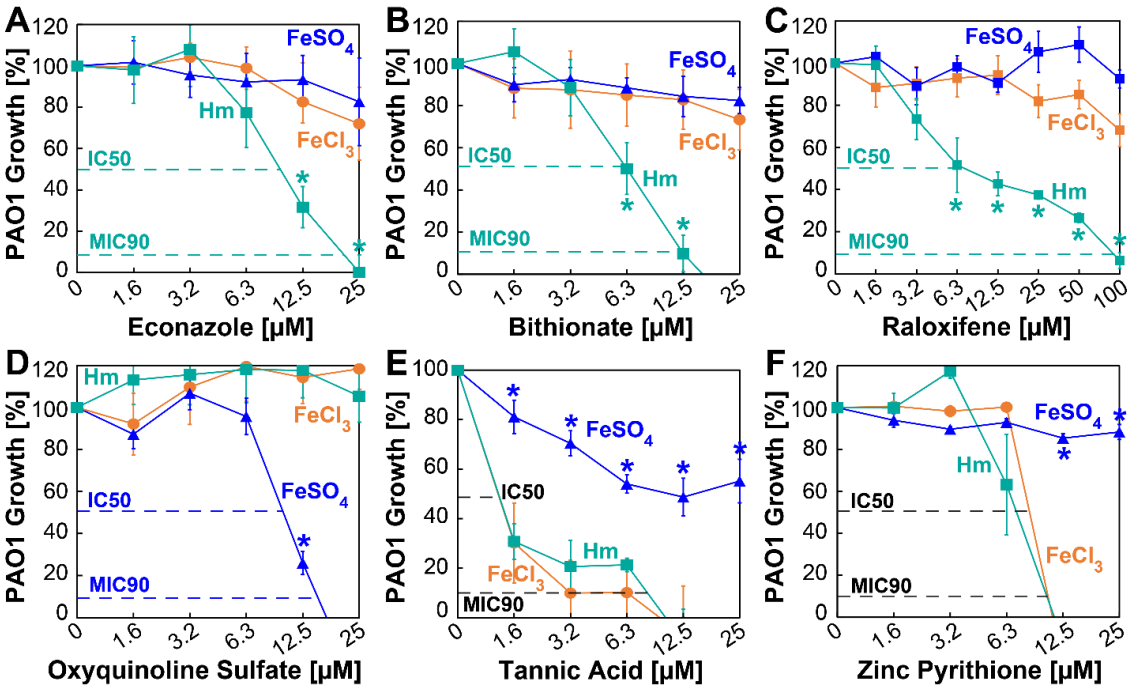

Figure 2.4. Specific activity of hit molecules determined by dose-response assays.
Survival of PAO1 in SMM-N containing 5 μM $FeCl_3$ (orange circles) or 5 μM Hm (cyan squares) or 5 μM $FeSO_4$ (blue triangles) in the presence of increasing concentrations of econazole **(A)**, bithionate **(B)**, raloxifene **(C)**, oxyquinoline sulfate **(D)**, tannic acid **(E)**, and zinc pyrithione **(F)**. PAO1 growth was monitored by measuring endpoint OD_{600} at 10 h and growth % was determined relative to growth of PAO1 in the absence of any hit molecules. Error bars represent SEM of five biological replicates. Growth data points with asterisks are significantly different from the growth in the other iron conditions. Significance was determined by Tukey's HSD following an *F*-test ($p<0.05$). Source data file is provided.

Activity of heme- and ferrous-specific inhibitors.

Utilization of Hm and ferrous iron invariably starts with their transport into the cell across the outer and inner membranes of *Pa* by specific membrane transporter proteins [75]. It is possible that these transporters are being blocked by HSI and FSI molecules preventing uptake of Hm and $FeSO_4$, respectively. Alternatively, it may be that the HSI and FSI molecules are directly binding Hm or $FeSO_4$, which prevents access of *Pa* to the iron source. If the molecules are blocking transporter proteins, we hypothesized that increasing the iron levels would not recover growth of *Pa*. If the inhibitors are preventing access to Hm and $FeSO_4$ through binding, we hypothesized that increasing the iron levels would then recover growth of *Pa*. To establish a possible mechanism, we determined the ability of the hit molecules to block *Pa* growth in the presence of increasing concentrations of Hm or $FeSO_4$. We only analyzed the hit molecules with MIC90 activity (econazole, bithionate and oxyquinoline sulfate). The antipseudomonal activity of econazole remains the same at 5 µM and 10 µM Hm (IC50 ~12.5 µM) and its activity increases (IC50 <12.5 µM) at 15 µM Hm (Fig. 2.5 A). Interestingly, the MIC90 for econazole decreases with increasing concentrations of Hm (Fig. 2.5 A). Antipseudomonal activity of bithionate remains the same at 5 µM and 10 µM with no statistically significant differences (Fig. 2.5 B), but at 15 µM Hm the antipseudomonal activity of bithionate is partially relieved with the IC50 increasing to ~10 µM, which was statistically significant (Fig. 2.5 B). These observations indicate that econazole and bithionate inhibit growth of *Pa* in a Hm-dependent manner but likely by different mechanisms. For the FSI oxyquinoline sulfate, there is only a marginal reduction (IC50 ~14 µM) in antipseudomonal activity after increasing $FeSO_4$ concentration to 10 µM and 15 µM (Fig. 2.5 C). However, the MIC90 for oxyquinoline sulfate mostly remains unchanged (Fig. 2.5 C) indicating that increasing the $FeSO_4$ concentration only marginally alleviates the $FeSO_4$-dependent antipseudomonal activity of oxyquinoline sulfate.

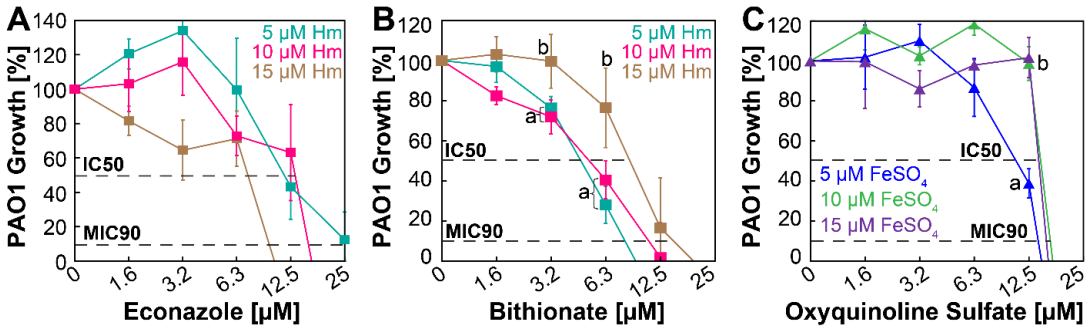

Figure 2.5. Effect of iron concentration on heme- and $FeSO_4$-specific inhibitors.
Survival of PAO1 in SMM-N containing 5 µM Hm (cyan) or 10 µM Hm (pink) or 15 µM Hm (brown) in the presence of increasing concentrations of econazole **(A)** or bithionate **(B)**. **C.** Survival of PAO1 in SMM containing 5 µM $FeSO_4$ (blue) or 10 µM $FeSO_4$ (green) or 15 µM $FeSO_4$ (purple) in the presence of increasing concentrations of oxyquinoline sulfate. PAO1 growth was monitored by measuring endpoint OD_{600} at 10 h and growth % was determined relative to growth of PAO1 in the absence of any hit molecules. Error bars represent SEM of five biological replicates. Plots with different letters are significantly different as determined by Tukey's HSD following an *F*-test ($p<0.05$). Source data file is provided.

Effect of HSI and FSI on meropenem activity.

A key aspect of antipseudomonal chemotherapy is to ensure that any lead molecules coming out of the drug discovery pipeline do not exhibit antagonistic effects on commercially used antibiotics. Since PAO1 is susceptible to meropenem in the nanomolar range (Fig. 2.3 B) and functions by inhibiting cell wall synthesis, we wanted to explore the effects of HSI and FSI molecules on the activity of meropenem. To this end, antipseudomonal activity of meropenem at varying concentrations was determined by growing PAO1 in the presence of 5 µM Hm and HSIs or 5 µM $FeSO_4$ and FSI. All HSI and FSI molecules were used at sub-inhibitory concentrations (3 µM) which is still in molar excess compared to the nanomolar concentrations of meropenem (Fig. 2.6). In the presence of the HSI bithionate, inhibitory activity of meropenem was completely unchanged against *Pa* (Fig. 2.6 A). In the presence of the HSI econazole, inhibitory activity of meropenem was slightly potentiated as growth of *Pa* was reduced at lower concentrations of meropenem (Fig. 2.6 A). However, this difference was not statistically significant. Interestingly, addition of the FSI oxyquinoline sulfate significantly potentiated the inhibitory activity of meropenem against *Pa*. The IC50 of meropenem is ~60 nM against *Pa* when grown in $FeSO_4$, but addition of oxyquinoline sulfate potentiates the inhibitory activity of meropenem by ~2-fold and reduces the IC50 to ~30 nM (Fig. 2.6 B). These results demonstrate that the iron-specific inhibitors identified from our HTS do not interfere with the activity of meropenem and that they can also potentiate the activity of meropenem.

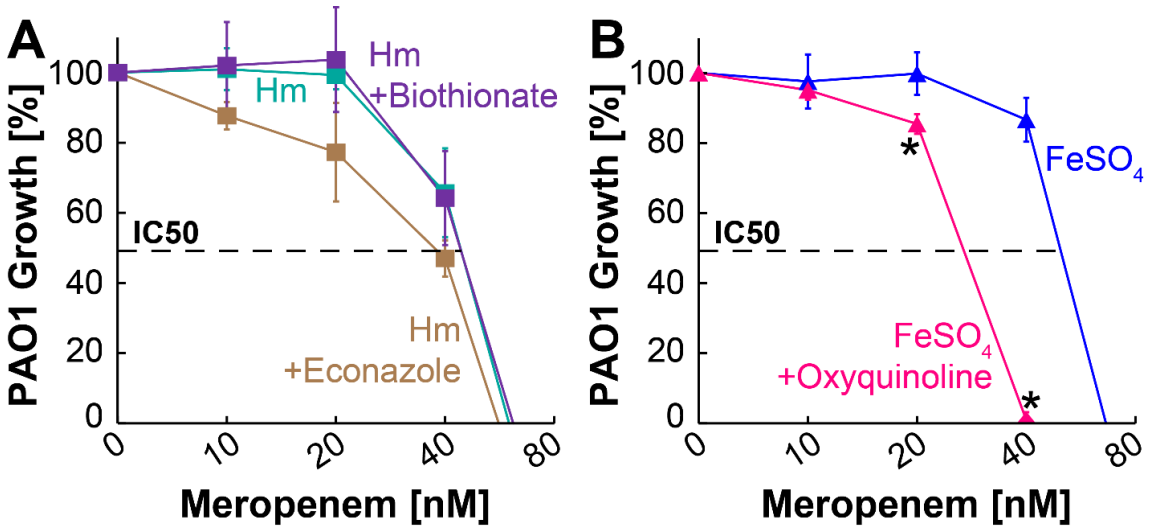

Figure 2.6. Effect of heme- and $FeSO_4$-specific inhibitors on activity of meropenem.
A. Survival of PAO1 in SMM-N containing 5 µM Hm (cyan) or 5 µM Hm and 3 µM econazole (brown) or 5 µM Hm and 3 µM bithionate (purple) in the presence of increasing concentrations of meropenem. **B.** Survival of PAO1 in SMM-N containing 5 µM $FeSO_4$ (blue) or 5 µM $FeSO_4$ and 3 µM oxyquinoline sulfate (pink) in the presence of increasing concentrations of meropenem. Asterisks denote significant differences as determined by Tukey's HSD following an *F*-test ($p<0.05$) compared to growth in just $FeSO_4$. ns denotes not significant. PAO1 growth was monitored by measuring endpoint OD_{600} at 10 h and growth % was determined relative to growth of PAO1 in the absence of any meropenem. Error bars represent SEM of five biological replicates. Note: Data points for Hm and $FeSO_4$ are the same as in Figure 2.3 B. Source data file is provided.

DISCUSSION

P. aeruginosa is strictly dependent on acquiring iron within the human host for survival and virulence because iron is an essential micronutrient required for vital biological processes [76]. *Pa* uses three redundant iron acquisition mechanisms to overcome iron limitation within the host: i) siderophore-mediated iron acquisition (SMIA) to chelate ferric (Fe^{3+}) iron from host Tf, Lf and F, ii) Hm-mediated iron acquisition (HIA) to sequester host Hm iron, and iii) ferrous-mediated iron acquisition (FIA) to directly transport ferrous (Fe^{2+}) iron. As stated previously, major efforts have been made to identify inhibitors of *Pa* SMIA, but research in identifying inhibitors of HIA and FIA is lacking. In this study we present proof-of-concept that a targeted whole cell screening approach can be employed to directly identify inhibitors of *Pa* HIA and FIA. We utilized a novel targeted conditional screening approach to identify molecules that specifically target and inhibit HIA and FIA of *Pa*. This approach relies on screening a small molecule library for antipseudomonal activity by growing *Pa* under different growth conditions, where the exogenously added iron source is the only variable in the medium. Each growth condition serves as a counter screen for the other to specifically identify either HIA or FIA inhibitors. We have termed these inhibitors as Hm-specific inhibitor (HSI) and ferrous-specific inhibitor (FSI), respectively. Utilizing this new approach, we identified three HSIs (econazole, bithionate and raloxifene), which only exhibit antipseudomonal activity in the presence of Hm iron, and one FSI (oxyquinoline sulfate), which only exhibits antipseudomonal activity in the presence of ferrous iron (Fig. 2.4). The iron-specific activity of these molecules is further supported by the observations that these molecules do not exhibit any antipseudomonal activity in the counter screening conditions.

We also attempted to determine a possible mechanism of action for the most active HSIs and FSI. Our results show that increasing the iron concentration in the medium only marginally

reduced or did not affect the antipseudomonal activity of these molecules (Fig. 2.5). This suggests that these inhibitors are likely not preventing access to the iron source through direct binding of Hm and ferrous iron, but this possibility cannot be discounted. It is well known that the primary mode of action of azole drugs such as econazole is mediated by binding the Hm cofactor [77] to inactivate cytochrome P450 enzymes, which are essential for diverse catalytic roles [78]. Since, *P. aeruginosa* has genes that encode P450 enzymes [79] and because it has been shown that econazole can bind these *Pa* P450 enzymes [80], it is possible that econazole could be inactivating the *Pa* P450 enzymes and inhibiting growth. If this was the case, then we would expect to also observe the antipseudomonal activity of econazole in the presence of $FeCl_3$ or $FeSO_4$ and not just specifically in the presence of Hm (Fig. 2.4 A). In *Pa*, outer membrane receptors first bind Hm and transport it into the periplasm, where Hm is bound by a substrate binding protein and then transported across the inner membrane by a dedicated ABC transporter [20]. It is conceivable that econazole could be binding to the protein-Hm complex at any point of this transport process and preventing Hm entry into the cytoplasm. Since increasing the Hm concentration did not alleviate the inhibitory activity of econazole, we speculate that econazole is likely blocking transport of Hm into the cytoplasm. The second HSI bithionate has higher antipseudomonal activity (IC50 ~6 µM, MIC90 ~12 µM) compared to econazole. Since increasing the Hm concentration to 15 µM in medium partially alleviated some antipseudomonal activity of bithionate, it may be that bithionate binds Hm and prevents access to Hm. We also identified raloxifene as another highly specific HSI but with much lower activity compared to econazole and bithionate. Interestingly, a previous study by Sui *et al.* identified raloxifene as an antipseudomonal that prevents production of pyocyanin [81], which is a siderophore required for ferric iron acquisition [20, 75]. The growth and infection assays in the Sui *et al.* study were performed with 100 µM raloxifene, which is the same

concentration where we observe ~30% inhibition in the presence of ferric chloride in our study (Fig. 2.4 C). However, our specific growth conditions clearly show raloxifene has much higher Hm-specific activity. To the best of our knowledge, our study is also the first to directly attempt to identify ferrous iron acquisition inhibitors and we show that oxyquinoline sulfate (OS) specifically inhibits growth of *Pa* in the presence of $FeSO_4$. OS and its derivatives are known antibacterial agents which can bind different metals [82-85] and has been shown to exhibit increased antibacterial activity in the presence of ferrous iron salts [86]. Based on these observations, it is likely that the antipseudomonal activity of OS is partially due to sequestration of ferrous iron because increasing $FeSO_4$ concentration from 5 µM to 10 µM allowed *Pa* to grow at 12.5 µM OS (Fig 2.5 C). On the same note increasing $FeSO_4$ concentration from 10 µM to 15 µM did not allow *Pa* to survive significantly better. In fact, for all $FeSO_4$ concentrations the MIC90 of OS was only marginally affected (Fig. 2.5 C) suggesting that OS may also be inhibiting growth by other mechanisms.

An unexpected finding of our HTS was the observation that tannic acid (TA) and zinc pyrithione (ZPT) inhibited growth of *Pa* both in the presence of $FeCl_3$ and Hm. Previous studies have shown that these molecules can be potent inhibitors of *Pa* both during planktonic and biofilm growth [87, 88]. Since TA and ZPT are known metal chelating compounds [89, 90], it is likely they inhibit *Pa* growth in $FeCl_3$ through ferric iron chelation. TA also forms ferrous iron complexes with lower affinity at neutral to alkaline pH. Our buffered (pH 6.8) growth medium may be allowing some Fe^{2+}-TA complexation, which could explain the partial growth defect observed in the $FeSO_4$ condition (Fig. 2.4 E). A more confounding observation is how TA and ZPT are inhibiting *Pa* growth in the presence of Hm. It is not known whether TA can bind and sequester Hm, and it is unlikely that TA can chelate iron from the porphyrin ring because porphyrin tightly

binds iron. The only known mechanisms of iron release from Hm is through cleavage of the porphyrin ring by dedicated heme monooxygenase enzymes [27]. On the other hand, there is a plausible explanation for ZPT-mediated Hm inhibition. ZPT is a commonly used antifungal and studies have shown that it inhibits yeast growth by inactivating iron-sulfur (Fe-S) proteins [91]. Since Fe-S cluster biogenesis is intimately linked to heme biogenesis and metabolism [92], this further leads to mitochondrial dysregulation and growth inhibition [93]. It is possible ZPT may be similarly impacting Fe-S proteins and heme metabolism in *Pa*. However, Fe-S proteins perform vital cellular functions under all conditions further raising the question of why the ZPT-mediated inhibition of Fe-S proteins would not inhibit *Pa* growth in the presence of $FeSO_4$. An alternative explanation could be that TA and ZPT are inhibiting some component(s) that is shared between ferric and heme iron acquisition pathways, which in this case would be the TonB-ExbBD proteins. Transport of Fe^{3+}-siderophore complex or Hm across the bacterial outer membrane is an active process requiring energy, which is provided by the TonB-ExbBD proteins [27]. Therefore, it is tempting to speculate that TA and ZPT could be inhibiting TonB-ExbBD function in some manner. Ferrous iron is transported by porins by passive diffusion in a TonB-independent manner and could explain the significantly reduced activity of TA and inactivity of ZPT in the presence of $FeSO_4$.

Altogether, the results of our study show that: i) our targeted whole cell HTS approach identifies molecules that block specific iron acquisition systems, ii) these iron-specific inhibitors are structurally diverse (Fig. 2.7), and iii) we can identify new roles for previously characterized iron inhibitors. There are some limitations to our current study. We recognize that one limitation is that molecules identified from this screen exhibit micromolar levels of antipseudomonal activity. We do not see this as a disadvantage because our primary goal was to show proof-of-concept for our targeted whole cell approach, and we successfully proved that our approach is logical and

performs robustly. We realize that antifungals such as econazole are cytotoxic and would not be used for actual chemotherapy. However, from this pilot screen we were able to identify structurally diverse molecules that can serve as a platform to rationally design or synthesize more targeted compound libraries for future high throughput screens. Another limitation of our study is that our screening was performed under very specific growth conditions. A reasonable argument could be made that the screening should have been performed in artificial sputum medium (ASM) which simulates the CF lung environment. To the best of our knowledge there are at least eight different ASM [66-73] that are used in CF research and the main drawback is that their iron source and levels cannot be manipulated. Our screening approach relies on exogenous addition of iron sources ($FeCl_3$, Hm or $FeSO_4$) to identify specific iron acquisition inhibitors. While chelex treatment can remove free iron from the ASM, it does not remove iron complexed in proteins and there is also risk of chelating other metals. For these reasons we opted to use a defined medium so that we could target specific iron acquisition systems. Furthermore, our screening was performed using the *Pa* PAO1 isolate, and it is possible that the small molecules identified in our screen could exhibit varying effects against other *Pa* isolates. We also recognize that our screening was performed with planktonically grown *Pa,* and it is well-established that *Pa* exists within biofilms where its metabolism is very different. An advantage of our approach is that it is highly adaptable to any growth condition and molecule screening can easily be performed against *Pa* grown within biofilms. While it was not within the scope of this study, we fully intend to use this screen to identify iron-specific inhibitors of *Pa* biofilms in future experiments.

A seminal study by Dr. Oglesby's group has shown that *Pa* mutants defective in siderophore production successfully colonize the CF lung and that *Pa* reduces siderophore production and upregulates the genetic components of heme and ferrous iron acquisition in the CF

lung [36]. These observations suggest that *Pa* preferentially uses heme and ferrous iron over ferric iron within the CF lung environment. Blocking iron acquisition systems simultaneously *in vivo* would starve *Pa* of an essential nutrient which could increase activity of other antipseudomonal antibiotics as we have shown is case with OS (Fig. 2.6 D). Our whole cell screening approach is advantageous because it directly identifies biologically active molecules that target heme and ferrous iron acquisition systems and overcomes the need for *in silico* designing of molecules based on structural analysis. Moreover, our screening approach to identify iron acquisition inhibitor is not just limited to *Pa* and can be easily extended to any pathogen. Since gram negative pathogens share many similarities in iron acquisition both at the mechanistic and molecular level [12, 14, 27, 64, 94-96], our screening approach presents a significant opportunity to develop novel broad spectrum iron acquisition inhibitors of gram negative pathogens, which pose an imminent global threat to human health [56, 97, 98]. In conclusion, we envision to identify highly active molecules that can be developed into a cocktail of iron acquisition inhibitors that can block SMIA, HIA and FIA not only in *Pseudomonas aeruginosa* but also in other gram-negative pathogens.

ACKNOWLEDGEMENTS
This study was supported in part by NIH grant P20GM134973, an NIH-funded program that was made possible by NIGMS, and Oklahoma State University College of Arts and Sciences startup funds awarded to A.M.

DATA AVAILABILITY
All source data files are provided and are also available to anyone upon request. All requests should be addressed to Dr. Avishek Mitra.

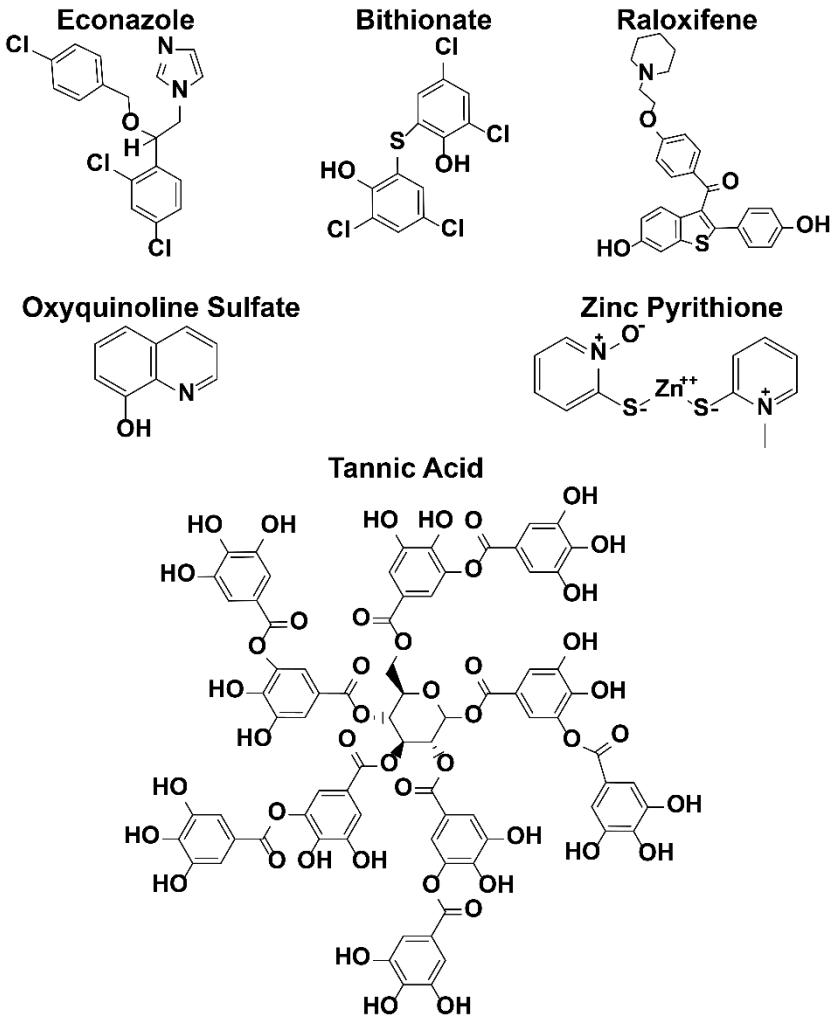

Figure 2.7. Structures of iron specific inhibitors identified from targeted whole cell high throughput screening assay.

Econazole, bithionate and raloxifene are heme specific inhibitors of *Pa*. Oxyquinoline sulfate is a ferrous-specific inhibitor of *Pa.* Zinc pyrithione and tannic acid inhibit growth of *Pa* in the presence of both ferric and heme iron.

CHAPTER III

CHARACTERIZING FERROUS SPECIFIC AND HEME SPECIFIC INHIBITORS AND THEIR MECHANISM OF ACTION.

3.1 Background

In our proof-of-concept HTS, we used the Pharmakon 1600 library, which consists of FDA-approved molecules. From this screen, we identified that econazole, bithionate and raloxifene exhibit antipseudomonal activity specifically in the presence of heme as an iron source. These molecules were named heme specific inhibitors, HSIs. Oxyquinoline sulfate exhibits antipseudomonal activity in the presence of ferrous iron and was designated as ferrous specific inhibitor (FSI). Econazole is an antifungal drug that is primarily applied topically, and, in some cases, it has been administered orally or intravenously [99]. Bithionate, often used in treating parasitic infections, inhibits electron transfer in the trematode, resulting in impaired anaerobic energy metabolism, eventually leading to the death of the trematode or parasite [100]. Raloxifene binds an estrogen receptor activating estrogenic pathways and is used to treat postmenopausal osteoporosis [101]. Oxyquinoline sulfate (OS) is an antiseptic drug with mild fungistatic and bacteriostatic activity and has metal chelating properties [102]. OS is used in various moisturizers such as Bag Balm and has a distinct color and smell.

In our proof-of-concept HTS we also identified two hits that fell into their own category. We identified ZPT and tannic acid that exhibit antipseudomonal activity in the presence of both heme and ferric iron simultaneously. Both tannic acid and ZPT show chelating activity [89]. Tannic acid is found in plants and certain foods and contains antioxidant properties. In addition,

tannic acid has exhibited antibacterial and antiviral properties [103]. ZPT, normally used to treat dandruff, has also shown antimicrobial activity [104]. Though each of these molecules are FDA approved and have mechanisms of action for treatment with certain illnesses or conditions, how these compounds work against *Pa* and the *Pa* iron acquisition systems have yet to be examined.

The overall objective of this study was to further characterize the activity of our hit molecules by determining: i) if the initial *Pa* cell inoculum affects activity of hit molecules, ii) if hit molecules bind heme or iron molecules, iii) if hit molecules exhibit any iron chelating activity and iv) if the hit molecules are also active against multi-drug resistant *Pa* isolates.

3.2 Methods

Determining effect of inoculum on hit molecule activity.

Wild-type (WT) PAO1 was streaked onto a solid LB agar plate and grown statically for 24 hours at 37ºC. Liquid cultures were then inoculated from a single colony and incubated, shaking overnight in 5 mL of LB broth, then inoculated in 10mL of LB broth at an initial OD_{600} of 0.05 to bring the cells to exponential phase incubated at 37ºC for 3.5-4 hours. After 3.5 hours, the cells were washed two times with PBS and resuspended in the iron-free medium mentioned above (SMM-N). The cells were then incubated for 3 hours at initial OD_{600} of 0.5 to deplete the cells completely of iron. When iron depletion was finished, the cells were once again washed with PBS and resuspended in SMM-N. The cells were then inoculated into 96-well plates at an initial OD_{600} of 0.01 and 0.1 in SMM containing the various iron sources. All plates were incubated at 37ºC with shaking and observed after 10 hours.

Determine if HSIs bind heme iron or protoporphyrin (PPIX) ring.

Stock solutions of each compound were made in 10 mL of DMSO to a final concentration of 20 mM (0.0635 g zinc pyrithione, 0.088 g econazole, 0.0712 g bithionate, 0.10 g raloxifene, 0.34 g tannic acid). Additionally, working solutions of heme and protoporphyrin were made in 10 mL of DMSO at a 5 µM 10 µM and 15 µM concentration from a 20 mM heme and 10 mM protoporphyrin stock.

In the 96-well plate, 5, 10 and 15 µM heme was added to wells containing increasing concentrations of either HSIs, tannic acid or ZPT. Then absorbance was read in a range of 200-800 nm using a BioTek Synergy plate reader. Similarly in a 96-well plate 5, 10 and 15 µM protoporphyrin IX (PPIX) was added to wells containing increasing concentrations of the HSIs,

tannic acid or ZPT. The absorbance was also read in a range of 200-800 nm using a Biotek Synergy plate reader.

Binding activity of HSIs and surprise hits using a Chrome Azurol S Assay (CAS)

Initial CAS stock solutions-

Hexadecyltrimethylammonium bromide (CTAB) was added to 50 mL of millipore water to a final concentration of 10 mM (0.182 g). In a separate glass container 100 µL of 10 M HCl and 0.027 g of $FeCl_3$ was added to 100 mL of millipore water for a final concentration of 1 mM $FeCl_3$ and 10 mM HCl. In a separate beaker 0.06 g of chrome azurol dye was added to 50 mL of millipore water. Finally, 6.5 mL of 10 M HCl and 4.3 g of anhydrous piperazine was added to 25 mL of millipore water.

CAS Assay preparation-

6 mL of the 10 mM CTAB stock was diluted in 40 mL of millipore water. Then in a separate beaker 1.5 mL of FeCl3-HCl stock was added to 7.5 mL of the 2 mM CAS dye stock to create a Fe-CAS solution. The Fe-CAS solution was slowly added to the 6 mL CTAB while stirring. Then slowly the 25 mL HCl-anhydrous piperazine stock solution was added to the Fe-CAS-CTAB solution. Finally, 0.101688 g 5-sulfosalicylic acid was added to the solution to a final concentration of 4 mM then the completed CAS solution was brought to a final volume of 100 mL.

In 96 well plates 100 µL CAS dye solution was added to increasing concentrations of each of the hit compounds. The plates were then wrapped in foil and left in a dark room for an hour at room temperature. After an hour, the absorbance of each plate was read at a wavelength of 630 nm. Increasing concentrations of EDTA were also used as a chelation control. Each hit compound was subtracted by its background absorbance to avoid any interference.

Examining the effect of hit molecules against clinical *Pa* isolates.

Dose response assays to determine activity of hit molecules against clinical isolates were performed as described before with slight modifications[105]. Since clinical isolates failed to grow in just SMM base medium, all clinical isolates were grown in iron-free succinate minimal medium supplemented with 0.5% casamino acids (SMM-N-CAA). SMM-N-CAA was prepared in 1 L of ultrapure millipore water using the following reagents: 0.01 g of EDTA, 0.6 g of KH_2PO_4, 0.9 g of K_2HPO_4, 1.0 g of NH_4Cl, 0.2 g of $MgSO_4\ 7H_2O$, 0.075 g of $CaCl_2\ 6H_2O$, 2.2 g of sodium succinate, 0.1 g of yeast extract, 2.0 mL of trace elements, 2.0 mL of a vitamin solution, 33.3 mL of a 15% casamino acid (CAA) solution to a final concentration of 0.5%, and 40 mM MOPS (pH 6.8). The 15% CAA solution was prepared initially with 100 mL of millipore water and 15 g of Acid Casein Peptone [Fisher Bioreagents]. The CAA solution was then chelated overnight using 5 g of Chelex100 and then filter sterilized. The trace elements and vitamin solution were prepared identically to that of the HTS. Initial growth experiments were done to determine the exponential phase in a rich media and complete iron depletion. Each clinical isolate was streaked onto a solid LB agar plate and grown statically for 24 hours at 37ºC. Liquid cultures were then inoculated from a single isolated colony and grown shaking at 200 rpm overnight in 5 mL of LB broth at 37ºC. Then the culture was inoculated in 10 mL of LB broth at an OD_{600} of 0.05 to bring the cells to exponential phase incubated at 37ºC for 4 hours. After 4 hours, the cells were washed twice with 10 mL of PBS and resuspended in 10 mL of SMM-N-CAA. The cells were then incubated overnight at initial OD_{600} of 0.5 to deplete the cells completely iron. Iron depleted clinical isolates were harvested and washed twice with 10 mL of PBS. The clinical isolate cells were then inoculated in three 96-well plates at an OD_{600} of 0.005 to a final volume of 200 µL in SMM-N-CAA containing each of the 15 µM iron sources (heme, ferrous, ferric) with a range of

concentrations of each inhibitor. All plates were incubated at 37ºC with shaking or static conditions and observed after 10 hours.

3.3 Results

Effects of inoculum on hit molecule activity.

As stated in the previous chapter, the HSIs, FSI, tannic acid and ZPT hit molecules could be binding to some cell surface receptor or transporter protein(s) and preventing access to the iron source thus inhibiting growth of *Pa*. If this was the case, then we reasoned that increasing the initial *Pa* cell inoculum amount in the dose-response assays would indirectly increase the amount of cell surface proteins and result in decreased activity of the hit molecules. To test this hypothesis, all dose-response assays were repeated with the hit molecules except *Pa* cells were inoculated at an initial OD_{600} of 0.1 instead of 0.01 as done previously, which resulted in 10-fold increase in cell inoculum. We also tested the effect of varying the iron concentrations on the antipseudomonal activity of these molecules.

Initially in 5 µM heme the increase in cells does not affect the antipseudomonal activity of econazole with a similar IC50 value between the two of around 15 µM (Fig. 3.1 A). However, at 10 µM there is a slight shift in IC50 value from ~25 µM to 50 µM though still a trend in antipseudomonal activity remains (Fig. 3.1 B). At 15 µM econazole the antipseudomonal activity decreases slightly with an IC50 of ~ 25 µM in the OD_{600} of 0.01 and an IC50 of ~35 µM at the OD_{600} of 0.1 though no growth recovery is seen (Fig. 3.1 C). These results suggest that increasing the inoculum of PAO1 minimally affects the antipseudomonal activity of econazole with no complete recovery of PAO1.

In the presence of bithionate we did see a shift in activity when increasing the cell count (Fig. 3.2 A-C). In 5 µM heme we see a shift of and IC50 value of 25 µM bithionate to 75 µM **(**Fig. 3.2 A). At 10 µM heme we see a smaller shift from the IC50 value 25 µM to ~50 µM (Fig. 3.2 B). Finally in the presences of 15 µM heme the IC50 value shifts from ~25 µM to 50 µM **(**Fig. 3.2 C). Although there is a larger shift in IC50 values, the antipseudomonal activity of bithionate remains with no growth recovery seen in the presence of bithionate.

Finally, with oxyquinoline sulfate we see almost full recovery of the cells when increasing the cell count in all three conditions (Fig. 3.3 A-C). In the presence of 5 µM $FeSO_4$ increasing the optical density to OD_{600} of 0.1 recovers the growth of PAO1 in the presence of oxyquinoline sulfate (Fig. 3.3 A). Similarly in 10 µM $FeSO_4$ there is a slight decrease in activity at 25 µM when increasing the optical density but overall growth of PAO1 is recovered when increasing OD_{600} to 0.1(Fig. 3.3 B). Finally in 15 µM $FeSO_4$ we see some activity present at 100 µM but overall recovery of growth as well when increasing OD_{600} to 0.1 (Fig. 3.3 C). Increasing PAO1 inoculum in the presence of oxyquinoline sulfate alleviates the antipseudomonal activity.

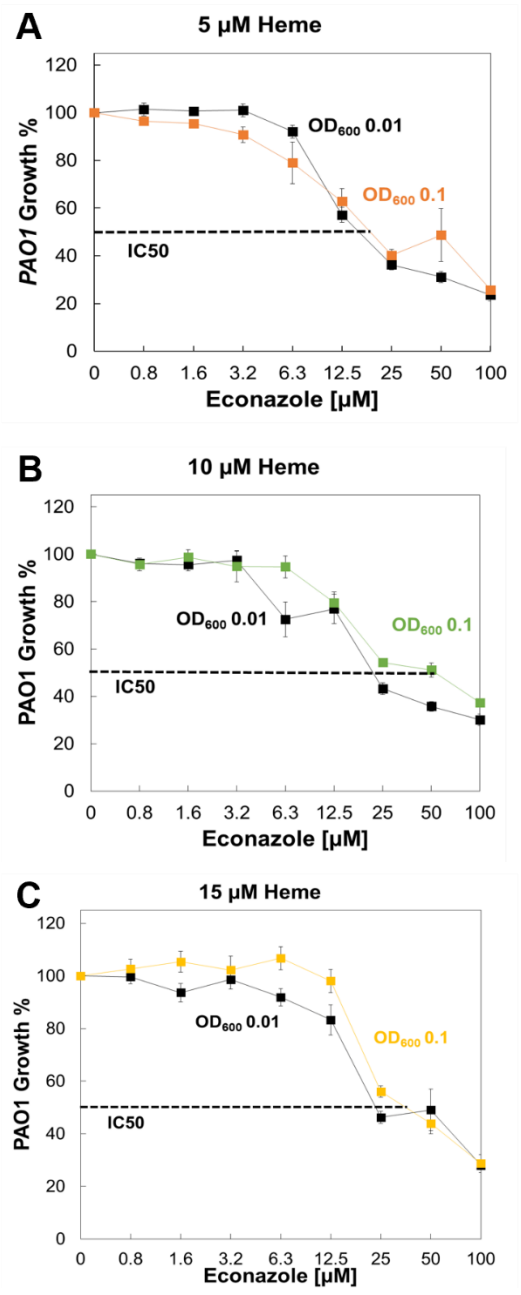

Figure 3.1. **Effect of increased inoculum on Econazole activity**

A. Survival of PAO1 in SMM-N containing increasing concentrations of econazole and 5 µM heme at a starting OD_{600} of 0.01 (black squares) or 5 µM heme (orange squares) at a starting OD_{600} of 0.1. **B.** Survival of PAO1 in SMM-N containing increasing concentrations of econazole and 10 µM heme at a starting OD_{600} of 0.01 (black squares) or 10 µM heme (green squares) at a starting OD_{600} of 0.1. **C.** Survival of PAO1 in SMM-N containing increasing concentrations of econazole and 15 µM heme at a starting OD_{600} of 0.01 (black squares) or 15 µM heme (yellow squares) at a starting OD_{600} of 0.1. Error bars represent SEM of five replicates.

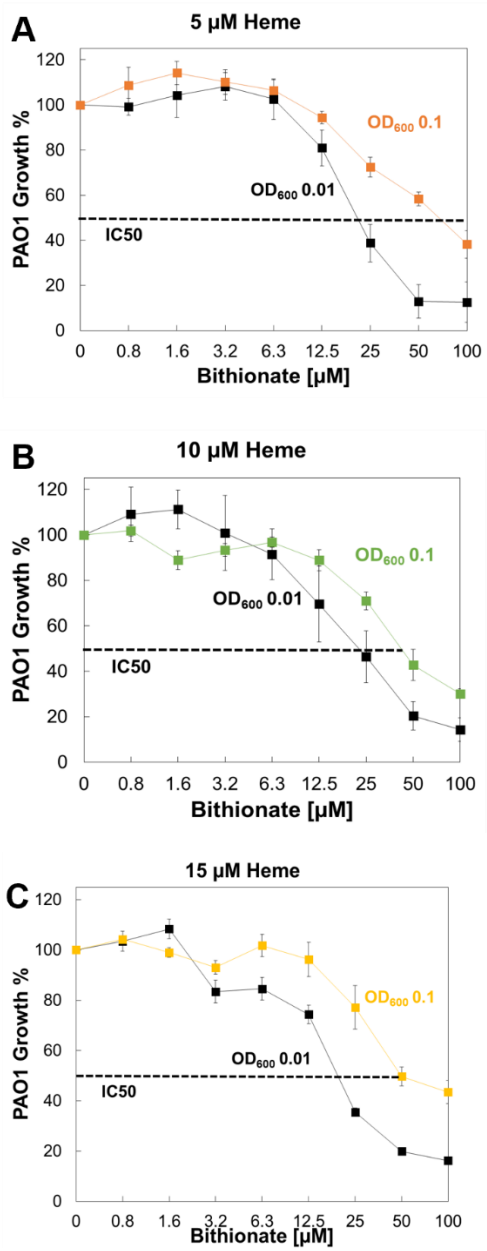

Figure 3.2. Effect of increased inoculum on Bithionate activity

A. Survival of PAO1 in SMM-N containing increasing concentrations of bithionate and 5 µM heme at a starting OD_{600} of 0.01 (black squares) or 5 µM heme (orange squares) at a starting OD_{600} of 0.1. **B.** Survival of PAO1 in SMM-N containing increasing concentrations of bithionate and 10 µM heme at a starting OD_{600} of 0.01 (black squares) or 10 µM heme (green squares) at a starting OD_{600} of 0.1. **C.** Survival of PAO1 in SMM-N containing increasing concentrations of bithionate and 15 µM heme at a starting OD_{600} of 0.01 (black squares) or 15 µM heme (yellow squares) at a starting OD_{600} of 0.1. Error bars represent SEM of five replicates.

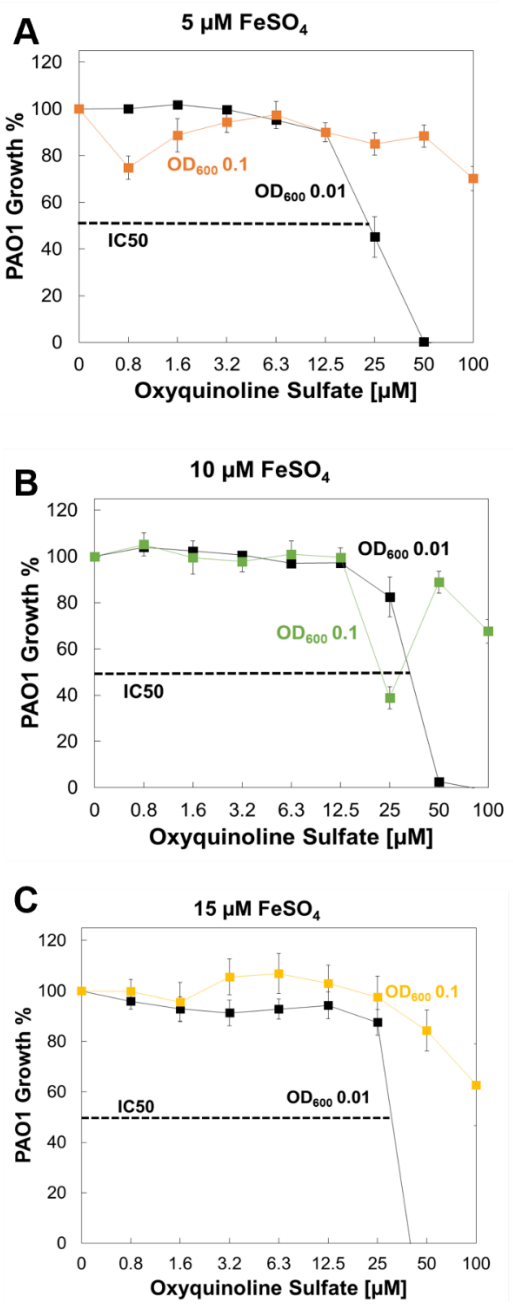

Figure 3.3. Effect of increased inoculum on Oxyquinoline Sulfate activity

A. Survival of PAO1 in SMM-N containing increasing concentrations of oxyquinoline sulfate and 5 µM $FeSO_4$ at a starting OD_{600} of 0.01 (black squares) or 5 µM $FeSO_4$ (orange squares) at a starting OD_{600} of 0.1. **B.** Survival of PAO1 in SMM-N containing increasing concentrations of oxyquinoline sulfate and 10 µM $FeSO_4$ at a starting OD_{600} of 0.01 (black squares) or 10 µM $FeSO_4$ (green squares) at a starting OD_{600} of 0.1. **C.** Survival of PAO1 in SMM-N containing increasing concentrations of oxyquinoline sulfate 15 µM $FeSO_4$ at a starting OD_{600} of 0.01 (black squares) or 15 µM $FeSO_4$ (yellow squares) at a starting OD_{600} of 0.1. Error bars represent SEM of five replicates.

Heme, Protoporphyrin (PPIX), and HSI absorbance experiments

As stated in the previous chapter, the HSIs, TA and ZPT hit molecules could be binding the heme molecule and preventing access to heme iron thus inhibiting growth of *Pa* in the presence of heme. To determine if these molecules are binding heme, we performed absorption spectroscopy experiments to detect specific changes in the heme absorbance spectrum. Heme has specific absorbance between 410-415 nm, which shifts upon being bound by other molecules. Thus, heme binding by the HSIs could be indirectly observed as a shift in the heme absorbance spectrum. It is possible that the HSIs could bind heme either by interacting with the iron atom in heme or by interacting with the protoporphyrin IX (PPIX) ring backbone. Since absorbance of heme primarily results from the PPIX backbone, we hypothesized if the molecules bind the PPIX backbone, then both heme and PPIX would show a similar shift in absorbance levels. If the molecules bind the iron atom, then only heme would show a shift in absorbance levels. As such, we also determined any possible PPIX-HSI interactions by similarly observing the absorbance spectrum of PPIX.

First, we measured the absorbance spectrum of different concentrations (5, 10 and 15 µM) of heme and PPIX to determine any differences in the spectra (Fig. 3.4). After confirming the differences in absorbance values between heme and PPIX they were compared with each of the concentrations of our HSIs and surprise hits. Each of the HSIs were examined in the presence of a constant concentration of heme or PPIX. The compounds were examined at 5, 10 and 15 µM heme and PPIX. Absorbance values for all compounds were examined around the IC50 values seen in the original HTS and compared against absorbance of either PPIX or heme without compound.

In 5 µM PPIX and heme in the presence of 12.5 µM econazole there is a similar shift in absorbance when compared to heme and PPIX without econazole (Fig. 3.5 A, B) suggesting econazole may be binding the PPIX backbone at 5 µM heme and PPIX. At 10 µM PPIX there is

a shift in absorbance in the presence of 12.5 µM econazole and no change in the heme absorbance values suggesting econazole is interacting with the PPIX backbone not the iron atom bound to heme at the 10 µM concentration (Fig. 3.5 C, D). Finally at the 15 µM PPIX and heme we see a large shift in PPIX absorbance at 12.5 µM PPIX but very minimal in heme again suggesting some interaction is occurring with econazole and the PPIX background (Fig. 3.5 E, F). Econazole most likely is not binding the iron molecule within heme due to the minimal absorbance changes observed in the heme conditions.

Bithionate shows similar absorbance trends to econazole in 5 µM PPIX with a shift in absorbance at 6.25 µM bithionate though in the presence of 5 µM heme no change in absorbance is seen (Fig. 3.6 A, B). This suggests at 5 µM PPIX there is interaction between the PPIX and bithionate backbone due to the large change in PPIX absorbance but none in heme. In 10 µM PPIX and heme there are similar trends in absorbance with an increase in both PPIX and heme in the presence of 6.25 µM bithionate. The 10 µM absorbance values suggest still an interaction between the PPIX backbone and bithionate (Fig. 3.6 C, D), if there was a shift in the heme absorbance values similar to that of the PPIX backbone without bithionate this would suggest binding of the iron molecule. At the 15 µM PPIX and heme absorbance values there are similar trends with minor change between the 0 µM bithionate and 6.25 µM bithionate values suggesting very little interaction is occurring between PPIX, heme and bithionate (Fig. 3.6 E, F). Similarly, econazole bithionate seems to be binding to the PPIX backbone rather than the iron molecule itself.

At 5 µM PPIX and heme there is a large shift in absorbance in the presence of 6.25 µM raloxifene again suggesting some interaction of raloxifene and the PPIX backbone due to the lack of shift in the heme absorbance values (Fig. 3.7 A, B). At 10 µM heme there is no shift in

absorbance but an increase in 10 µM PPIX in the presence of 6.25 µM raloxifene with binding occurring most likely in the PPIX backbone (Fig. 3.7 C, D). The absorbance values at 15 µM PPIX and heme are almost identical with no change when compared to the 0 µM raloxifene absorbance (Fig. 3.7 E, F). Raloxifene, like both econazole and raloxifene most likely is not binding the iron molecule within heme but rather binding some component of the PPIX backbone.

Finally tannic acid and zinc pyrithione the surprise hits show very minimal shifts in absorbance in both PPIX and heme. Tannic acid shows no shift at 5 and 15 µM PPIX and heme with all absorbance values matching the values of absorbance with no compound present (Fig. 3.8 A, B and E, F). However, at 10 µM PPIX and heme there is a slight increase in absorbance in the presence of 1.56 µM tannic acid suggesting some small interaction of tannic acid and the PPIX backbone (Fig. 3.8 C, D). With ZPT there is an increase in absorbance in the 5 and 15 µM PPIX and heme values indicating there is no binding of the iron molecule but rather some interaction with the backbone again (Fig. 3.9 A, B and E, F). At 10 µM PPIX there is no change in absorbance values but an increase in 10 µM heme absorbance (Fig. 3.9 C, D). Though the majority of the HSIs and surprise hits suggest an interaction or binding of the PPIX backbone rather than binding to the iron molecule within heme itself, more investigation of this interaction is needed.

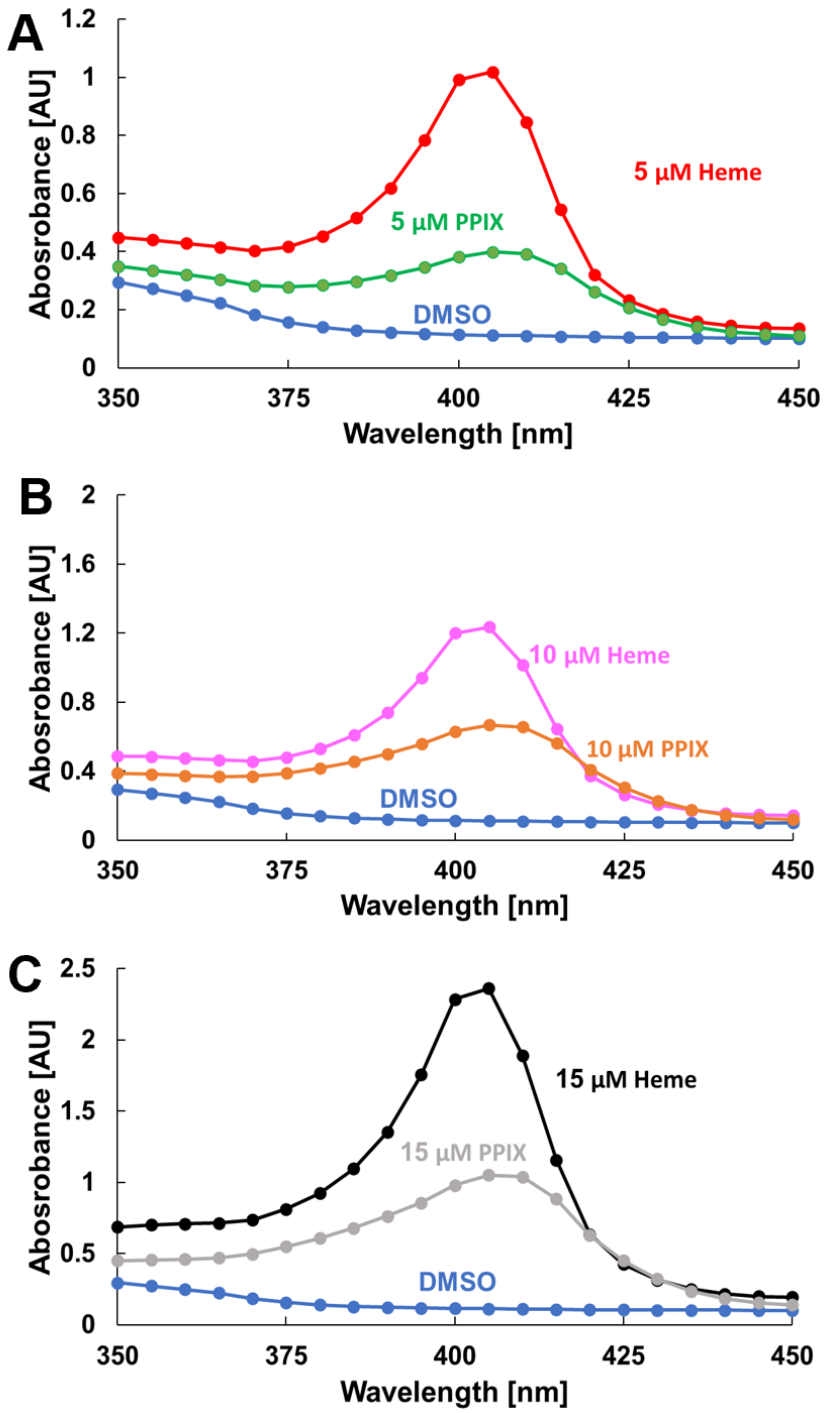

Figure 3.4. Initial heme and PPIX absorbance experiments-
A. 5 µM heme and 5 µM PPIX absorbance values comparison for validation. **B.** 10 µM heme and 10 µM PPIX absorbance values comparison for validation. **C.** 15 µM heme and 15 µM PPIX absorbance values comparison for validation.

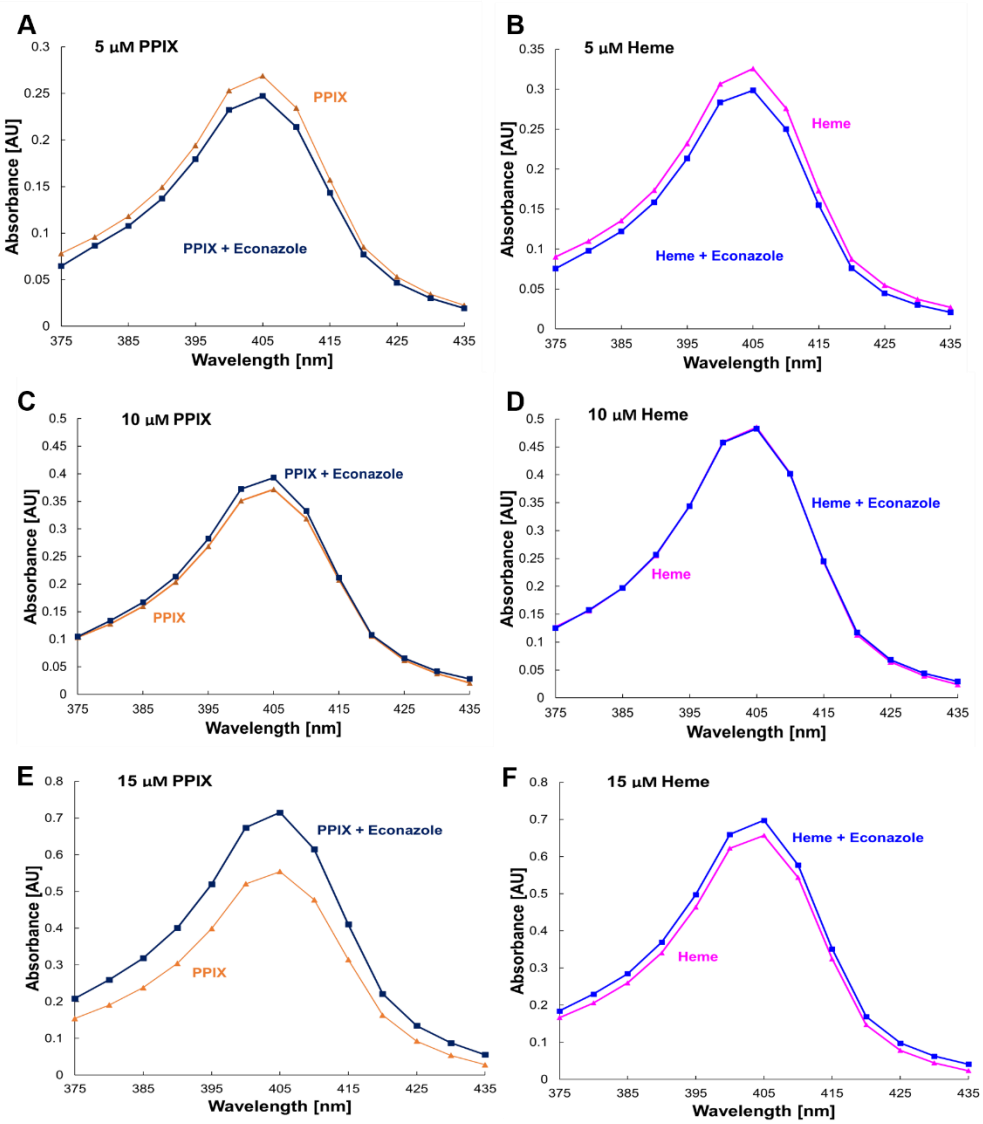

Figure 3.5. Changes in absorbance of PPIX and heme in the presence of Econazole- **A.** Absorbance of 5 µM PPIX with no added econazole (orange triangles) and absorbance of 5 µM PPIX with 12.5 µM econazole (dark blue squares). **B.** Absorbance of 5 µM heme with no added econazole (pink triangles) and absorbance of 5 µM heme with 12.5 µM econazole (blue squares). **C.** Absorbance of 10 µM PPIX with no added econazole (orange triangles) and absorbance of 10 µM PPIX with 12.5 µM econazole (dark blue squares). **D.** Absorbance of 10 µM heme with no added econazole (pink triangles) and absorbance of 10 µM heme with 12.5 µM econazole (blue squares). **E.** Absorbance of 15 µM PPIX with no added econazole (orange triangles) and absorbance of 15 µM PPIX with 12.5 µM econazole (dark blue squares). **F.** Absorbance of 15 µM heme with no added econazole (pink triangles) and absorbance of 15 µM heme with 12.5 µM econazole (blue squares). All absorbance values are subtracted from background absorbance of compound in DMSO at each concentration.

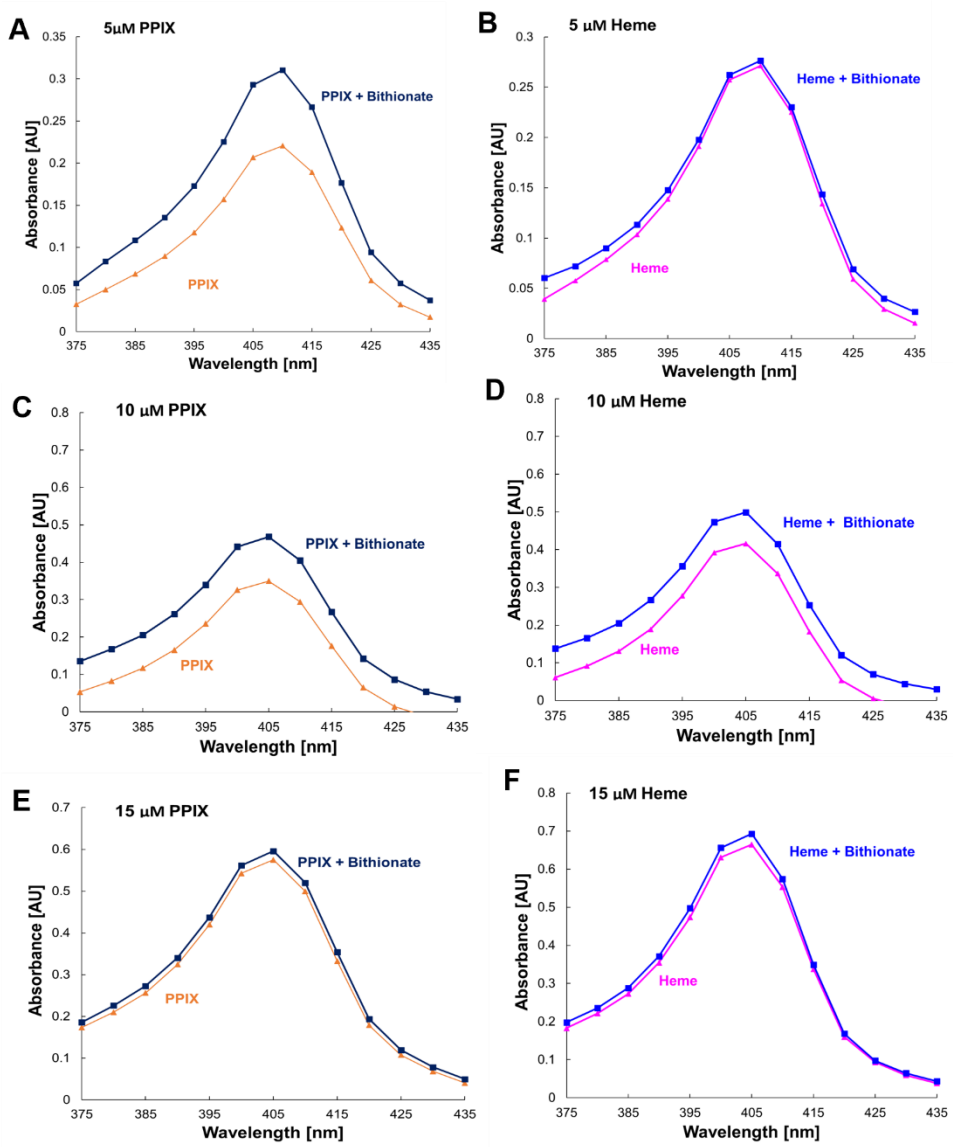

Figure 3.6. Changes in absorbance of PPIX and heme in the presence of Bithionate- **A.** Absorbance of 5 µM PPIX with no added bithionate (orange triangles) and absorbance of 5 µM PPIX with 6.25 µM bithionate (dark blue squares). **B.** Absorbance of 5 µM heme with no added bithionate (pink triangles) and absorbance of 5 µM heme with 6.25 µM bithionate (blue squares). **C.** Absorbance of 10 µM PPIX with no added bithionate (orange triangles) and absorbance of 10 µM PPIX with 6.25 µM bithionate (dark blue squares). **D.** Absorbance of 10 µM heme with no added bithionate (pink triangles) and absorbance of 10 µM heme with 6.25 µM bithionate (blue squares). **E.** Absorbance of 15 µM PPIX with no added bithionate (orange triangles) and absorbance of 15 µM PPIX with 6.25 µM bithionate (dark blue squares). **F.** Absorbance of 15 µM heme with no added bithionate (pink triangles) and absorbance of 15 µM heme with 6.25 µM bithionate (blue squares). All absorbance values are subtracted from background absorbance of compound in DMSO at each concentration.

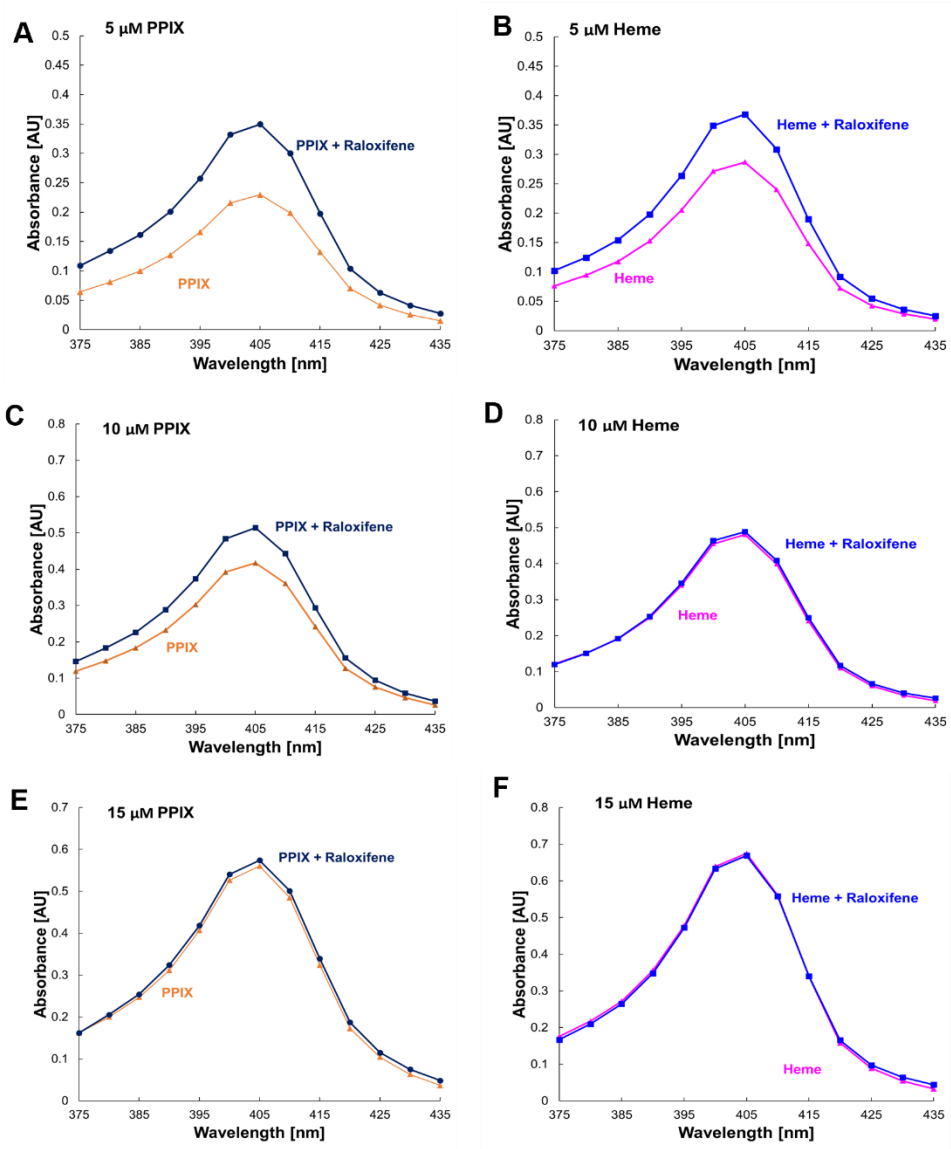

Figure 3.7. Changes in absorbance of heme and PPIX in the presence of Raloxifene- **A.** Absorbance of 5 µM PPIX with no added raloxifene (orange triangles) and absorbance of 5 µM PPIX with 6.25 µM raloxifene (dark blue squares). **B.** Absorbance of 5 µM heme with no added raloxifene (pink triangles) and absorbance of 5 µM heme with 6.25 µM raloxifene (blue squares). **C.** Absorbance of 10 µM PPIX with no added raloxifene (orange triangles) and absorbance of 10 µM PPIX with 6.25 µM raloxifene (dark blue squares). **D.** Absorbance of 10 µM heme with no added raloxifene (pink triangles) and absorbance of 10 µM heme with 6.25 µM raloxifene (blue squares). **E.** Absorbance of 15 µM PPIX with no added raloxifene (orange triangles) and absorbance of 15 µM PPIX with 6.25 µM raloxifene (dark blue squares). **F.** Absorbance of 15 µM heme with no added raloxifene (pink triangles) and absorbance of 15 µM heme with 6.25 µM raloxifene (blue squares). All absorbance values are subtracted from background absorbance of compound in DMSO at each concentration.

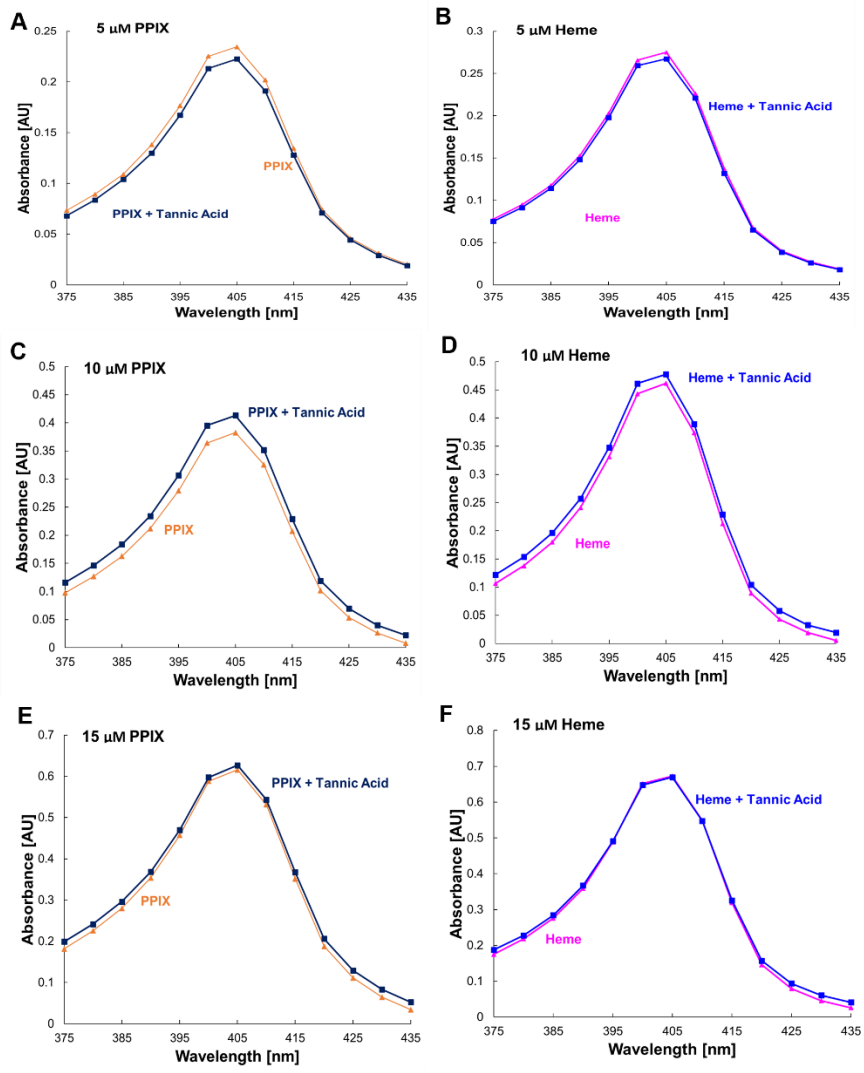

Figure 3.8. Changes in absorbance of heme and PPIX in the presence of Tannic Acid- **A.** Absorbance of 5 µM PPIX with no added tannic acid (orange triangles) and absorbance of 5 µM PPIX with 1.56 µM tannic acid (dark blue squares). **B.** Absorbance of 5 µM heme with no added tannic acid (pink triangles) and absorbance of 5 µM heme with 1.56 µM tannic acid (blue squares). **C.** Absorbance of 10 µM PPIX with no added tannic acid (orange triangles) and absorbance of 10 µM PPIX with 1.56 µM tannic acid (dark blue squares). **D.** Absorbance of 10 µM heme with no added tannic acid (pink triangles) and absorbance of 10 µM heme with 1.56 µM tannic acid (blue squares). **E.** Absorbance of 15 µM PPIX with no added tannic acid (orange triangles) and absorbance of 15 µM PPIX with 1.56 µM tannic acid (dark blue squares). **F.** Absorbance of 15 µM heme with no added tannic acid (pink triangles) and absorbance of 15 µM heme with 1.56 µM tannic acid (blue squares). All absorbance values are subtracted from background absorbance of compound in DMSO at each concentration.

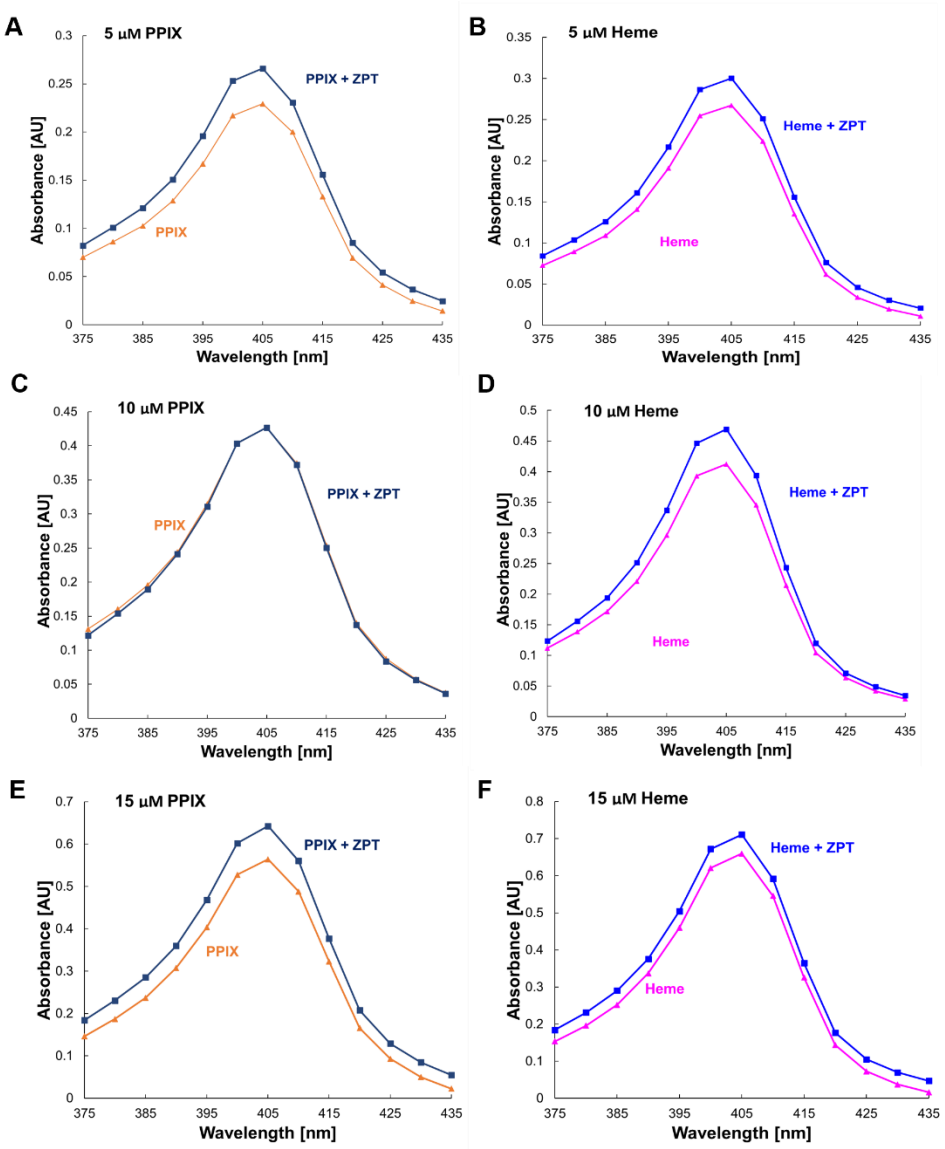

Figure 3.9. Changes in absorbance of heme and PPIX in the presence of Zinc Pyrithione- **A.** Absorbance of 5 µM PPIX with no added ZPT (orange triangles) and absorbance of 5 µM PPIX with 12.5 µM ZPT (dark blue squares). **B.** Absorbance of 5 µM heme with no added ZPT (pink triangles) and absorbance of 5 µM heme with 12.5 µM ZPT (blue squares). **C.** Absorbance of 10 µM PPIX with no added ZPT (orange triangles) and absorbance of 10 µM PPIX with 12.5 µM ZPT (dark blue squares). **D.** Absorbance of 10 µM heme with no added ZPT (pink triangles) and absorbance of 10 µM heme with 12.5 µM ZPT (blue squares). **E.** Absorbance of 15 µM PPIX with no added ZPT (orange triangles) and absorbance of 15 µM PPIX with 12.5 µM ZPT (dark blue squares). **F.** Absorbance of 15 µM heme with no added ZPT (pink triangles) and absorbance of 15 µM heme with 12.5 µM ZPT (blue squares). All absorbance values are subtracted from background absorbance of compound in DMSO at each concentration.

Determining iron chelating properties of hit molecules by CAS Assay.

It is possible that the hit molecules could be directly chelating iron which subsequently reduces iron availability and inhibits growth of *Pa*. We determined iron chelating properties of our hit molecules by performing the Chrome Azurol S (CAS) assay. In principle, the CAS dye is complexed with ferric iron and this complex exhibits a blue color which can be quantified by measuring absorbance at 630 nm. In the presence of an iron chelator, iron is removed from the complex which shifts the color to orange and reduces absorbance at 630 nm. This principle allows both quantitative and qualitative determination of iron chelating properties of small molecules.

Using EDTA as a control chelator, we measured the change in CAS absorbance at 630nm in the presence of our hit compounds. Each of the three HSIs at concentrations used in the HTS exhibited little to no absorbance change compared to EDTA in the presence of the CAS complex (Fig. 3.10 A, B, C). Thus, these compounds are not chelating iron (III), though not surprising when considering these are heme-specific compounds. When moving to the FSI oxyquinoline sulfate, there is a shift in absorbance values, not to the levels of EDTA but significant (Fig. 3.10 D). Oxyquinoline sulfate is a known metal chelator so it is possible we are seeing slight chelation of the Fe (III) bound within the CAS complex [102]. Finally, tannic acid and ZPT, when exposed to the CAS assay, both exhibited activity in heme and ferric conditions in our original HTS. Tannic acid showed solid chelating activity when compared to EDTA, where ZPT showed little to no chelating activity. From these experiments, we can conclude that some chelation activity is present in oxyquinoline sulfate and a large amount in tannic acid. It is possible that oxyquinoline sulfate and tannic acid are chelating ferric iron resulting in a reduction of iron availability in *Pa*. However, more investigation is needed as to what exactly is occurring.

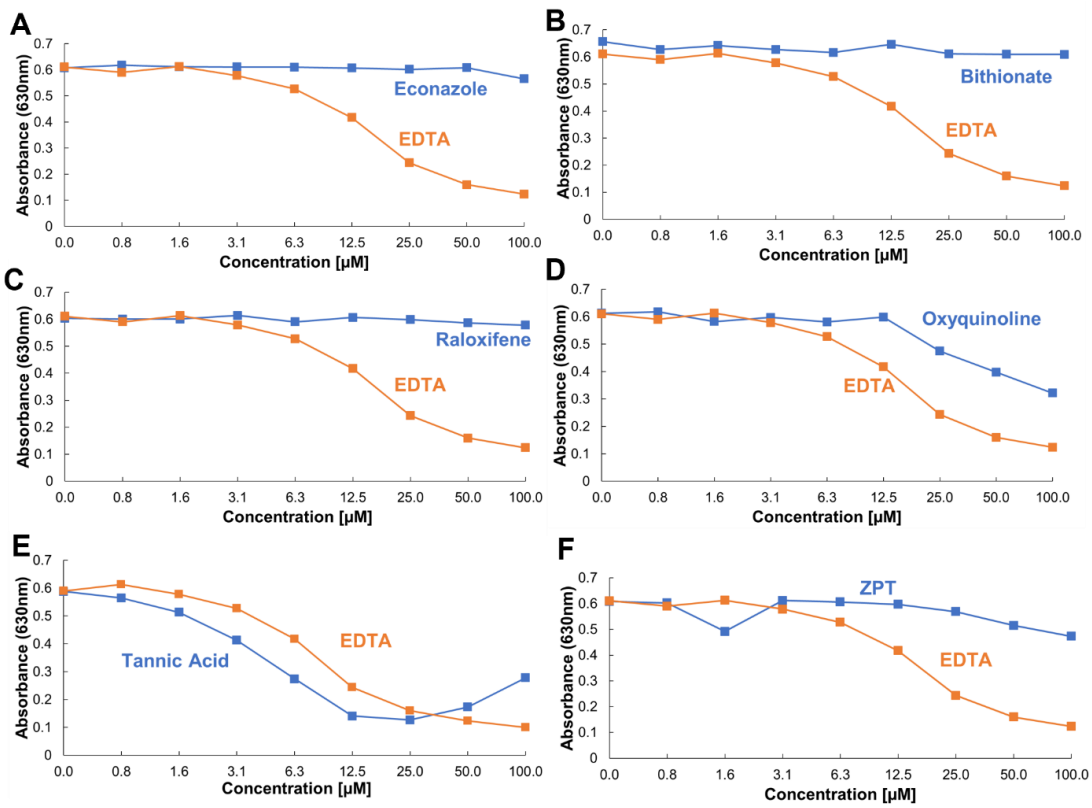

Figure 3.10. Chrome Azurol S Assay-
A B and C. HSI hits (blue squares) compared to a known chelator EDTA (orange squares) **D.** Oxyquinoline Sulfate (blue squares) compared to EDTA (orange squares) **E.** Tannic acid (blue squares) compared to EDTA (orange squares). **F.** Zinc pyrithione (ZPT) (blue squares) compared to EDTA (orange squares).

Determining activity of hit molecules against *Pa* clinical isolates.

Our HTS was performed using the PAO1 lab strains. For any of these molecules to become potential antipseudomonal agents, they must ideally exhibit activity again clinical *Pa* isolates which are typically drug-resistant and have innate abilities to efflux antibiotics. Thus, we wanted to determine if the hit molecules identified from our screen are also active against *Pa* clinical isolates. To this end, four clinical isolates were obtained from Dr. Erika Lutter at Oklahoma State University and used to determine the activity of our hit molecules. Clinical isolates were initially cultured in LB and then iron-depleted in SMM-N as performed with PAO1. All four clinical isolates were grown in 10mL of LB for around 4 hours; each isolate taking longer to reach the exponential phase than PAO1 (Fig. 3.11). The clinical isolates, however, did not grow in the SMM-N media used in our initial screen. Supplementation of SMM-N media with casamino acids (CAA) at 0.5% final concentration allowed all clinical strains to grow efficiently. As such, clinical isolates were routinely iron-depleted in SMM-N-CAA and hit molecule activity against isolates was determined in dose-response assays in SMM-N-CAA containing specific iron sources (ferric chloride, heme, or ferrous sulfate), just as we did previously. In our previous study, all dose-response assays were performed with planktonically grown cultures. Since there are metabolic differences in cultures grown planktonically and statically, we also determined activity of our hit molecules against statically grown cultures.

The first clinical isolate, *5715d*, was screened with each of the HSIs and FSI (Fig 3.12). Across each of the compounds, there was no specific activity in any of the iron sources with varying activity in all three iron conditions. Some of the compounds showed minor inhibition in all three iron sources (Fig. 3.12 C, D, G, H). However, the next clinical isolate *112014b* showed activity in many of our hit compounds. Dose response curves indicated an IC50 of ~75 µM for

econazole in both shaking and static conditions (Fig. 3.13 A, B) while remaining inactive in ferrous sulfate and ferric chloride. No specific activity was seen in bithionate (Fig. 3.13 C, D) while in raloxifene the IC50 value was ~75 µM in shaking and 50 µM in static (Fig. 3.13 E, F**)** again only exhibiting activity in heme. Dose response curves for the FSI oxyquinoline sulfate indicated an IC50 of close to 100 µM.

The third clinical isolate examined *3614b* also showed activity in econazole both in shaking and static conditions (Fig. 3.14 A, B) with IC50 values of ~60 µM in shaking and 50 µMin static conditions. Bithionate showed no specific activity against *3614b* (Fig. 3.14 C, D). Against raloxifene only minor activity was seen in the shaking condition with an IC50 of 100 µM (Fig. 3.14 E) however in the static condition a larger amount of activity was seen at an IC50 value of 12.5 µM (Fig. 3.14 F). Finally, oxyquinoline sulfate showed remarkably similar activity in both shaking and static conditions with an IC50 of 50 µM in both conditions (Fig. 3.14 G, H).

The final clinical isolate *9414d* again showed specific activity in econazole both in shaking and static conditions with IC50 values of 50 µM (Fig. 3.15 A, B) while no specific activity was seen in bithionate again (Fig. 3.15 C, D). Raloxifene showed significant inhibitory activity in heme in both shaking with an IC50 of 100 µM and static conditions with an IC50 value of ~45 µM with no activity present in ferrous sulfate or ferric chloride (Fig. 3.15 E, F). Oxyquinoline sulfate showed different activity in shaking versus static. In the shaking conditions activity was not seen until over 50 µM was present with an IC50 of 100 µM, however in the static condition inhibition is seen after 12.5 µM with an IC50 of ~30 µM (Fig. 3.15 G, H).

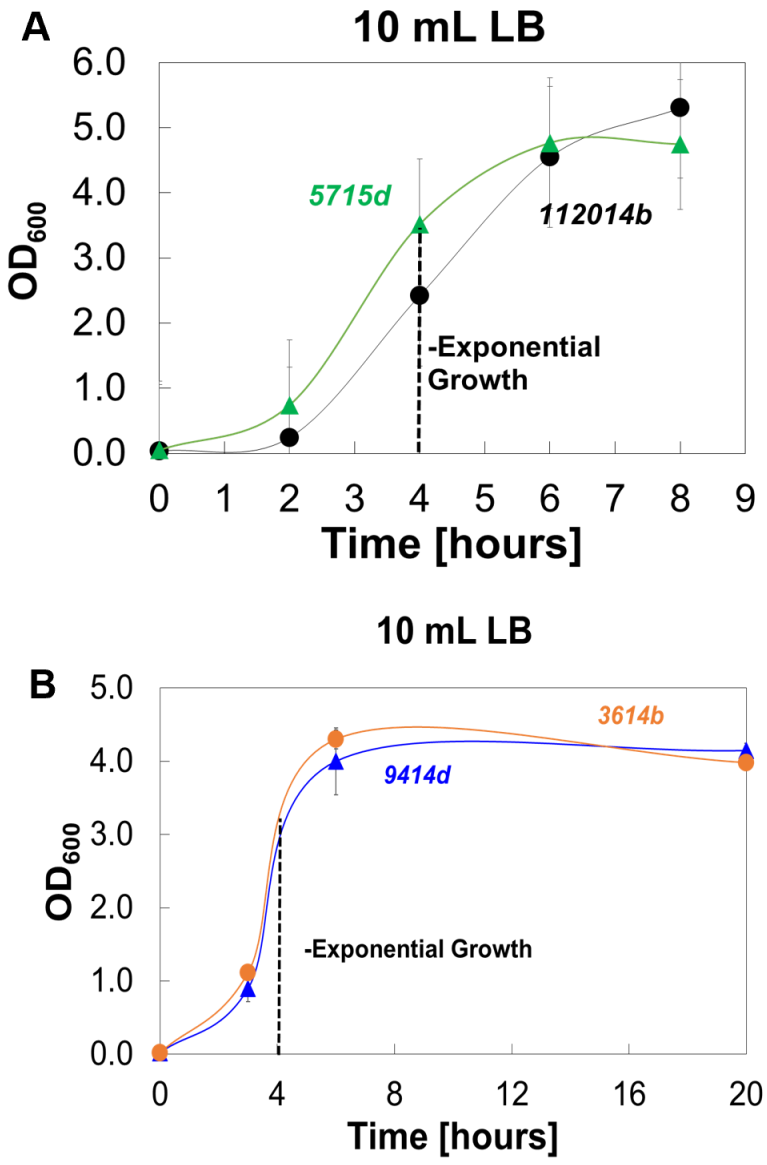

Figure 3.11. Initial Growth of Clinical Isolates in LB
A. Growth of clinical isolates *5715d* and *112014b* in LB to determine exponential and stationary growth phase. B. Growth of clinical isolates *9414d* and *3614b* in LB to determine exponential and stationary growth phase. Error bars represent standard error of mean (SEM) of three biological replicates. In many cases error bars are smaller than marker data points.

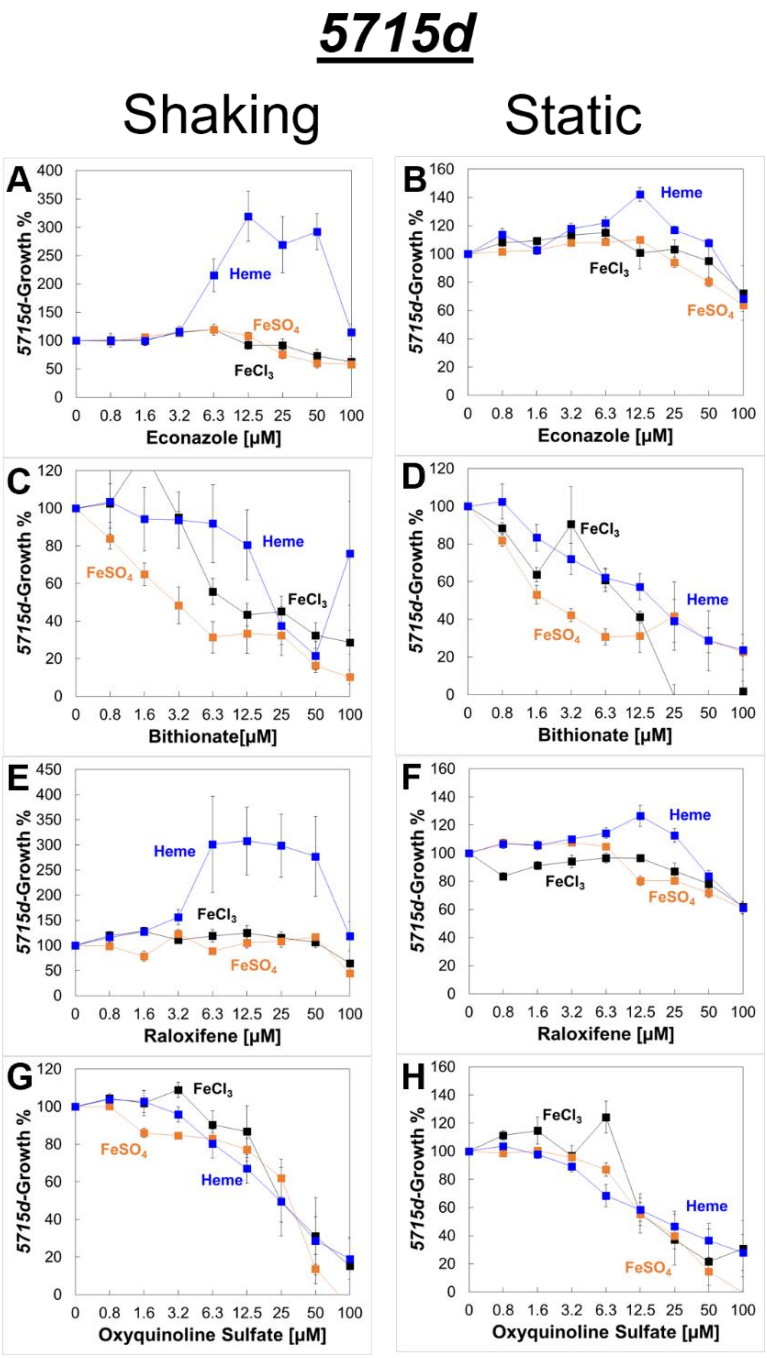

Figure 3.12. ***5715d*** **Shaking and Static growth experiments-**
Survival of 5715d in SMM-CAA containing 15 µM $FeCl_3$ (black squares) or 15 µM heme (blue squares) or 15 µM $FeSO_4$ (orange squares) with increasing concentrations of econazole (**A, B)** bithionate (**C, D)** raloxifene **(E, F)** and oxyquinoline sulfate **(G, H)** Growth of the clinical isolate was measured at endpoint OD_{600} at 10 hours with growth percentage determined by relative growth of isolate in the absence of any hit molecules. Error bars represent SEM of five replicates.

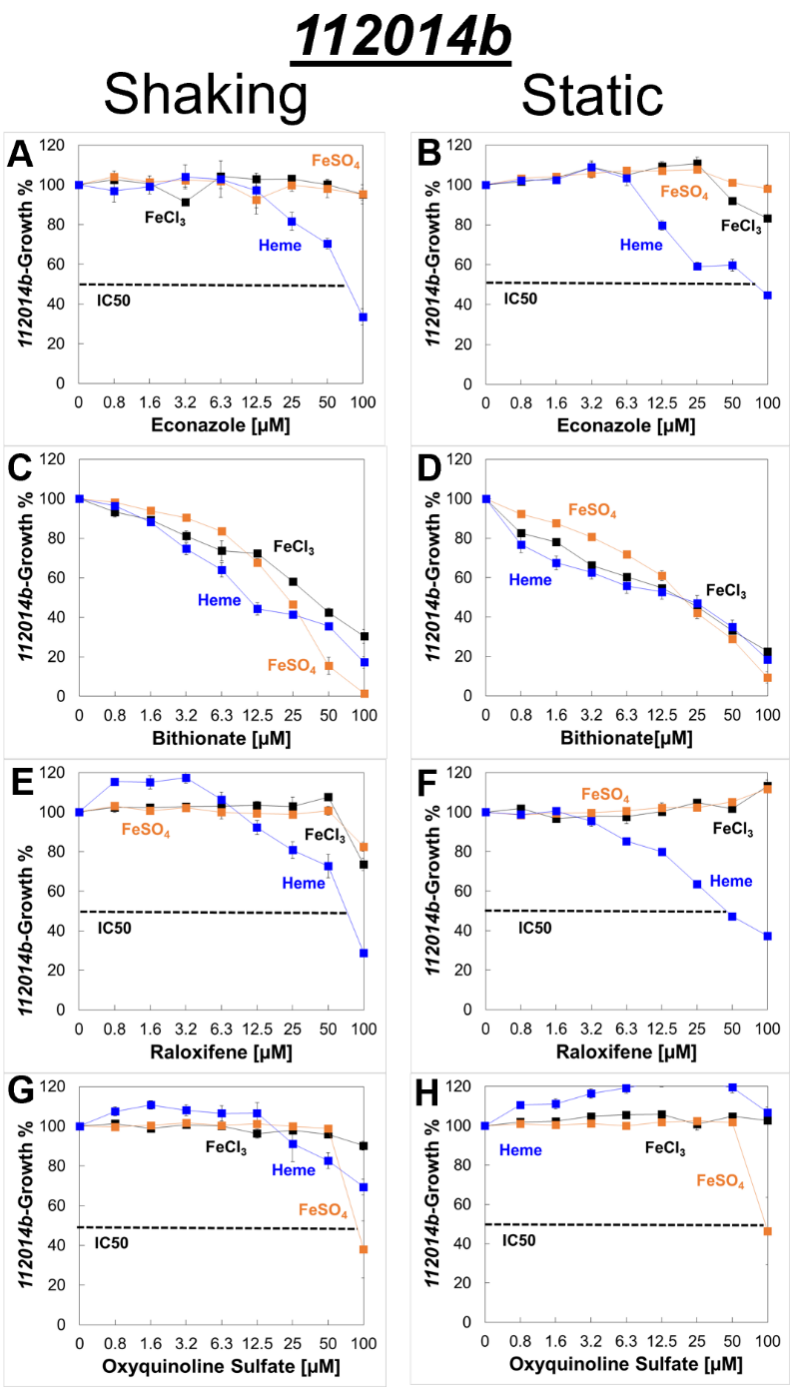

Figure 3.13. *112014b* Shaking and Static growth experiments-
Survival of *112014b* in SMM-CAA containing 15 μM $FeCl_3$ (black squares) or 15 μM heme (blue squares) or 15 μM $FeSO_4$ (orange squares) with increasing concentrations of econazole (**A, B)** bithionate (**C, D)** raloxifene **(E, F)** and oxyquinoline sulfate (**G, H).** Growth of the clinical isolate was measured at endpoint OD_{600} at 10 hours with growth percentage determined by relative growth of isolate in the absence of any hit molecules. Error bars represent SEM of five replicates.

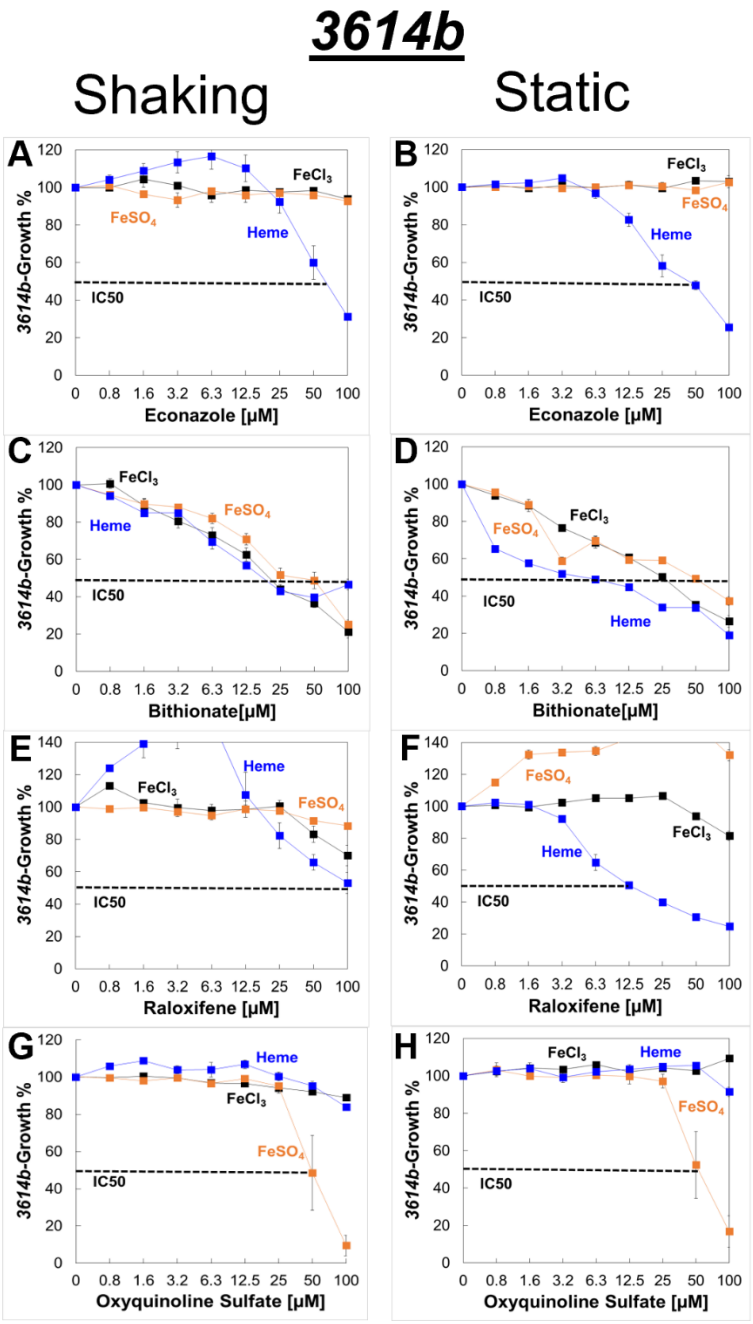

Figure 3.14. *3614b* Shaking and Static growth experiments-
Survival of *3614b* in SMM-CAA containing 15 μM $FeCl_3$ (black squares) or 15 μM heme (blue squares) or 15 μM $FeSO_4$ (orange squares) with increasing concentrations of econazole (**A, B)** bithionate (**C, D)** raloxifene **(E, F)** and oxyquinoline sulfate **(G, H)** Growth of the clinical isolate was measured at endpoint OD_{600} at 10 hours with growth percentage determined by relative growth of isolate in the absence of any hit molecules. Error bars represent SEM of five replicates.

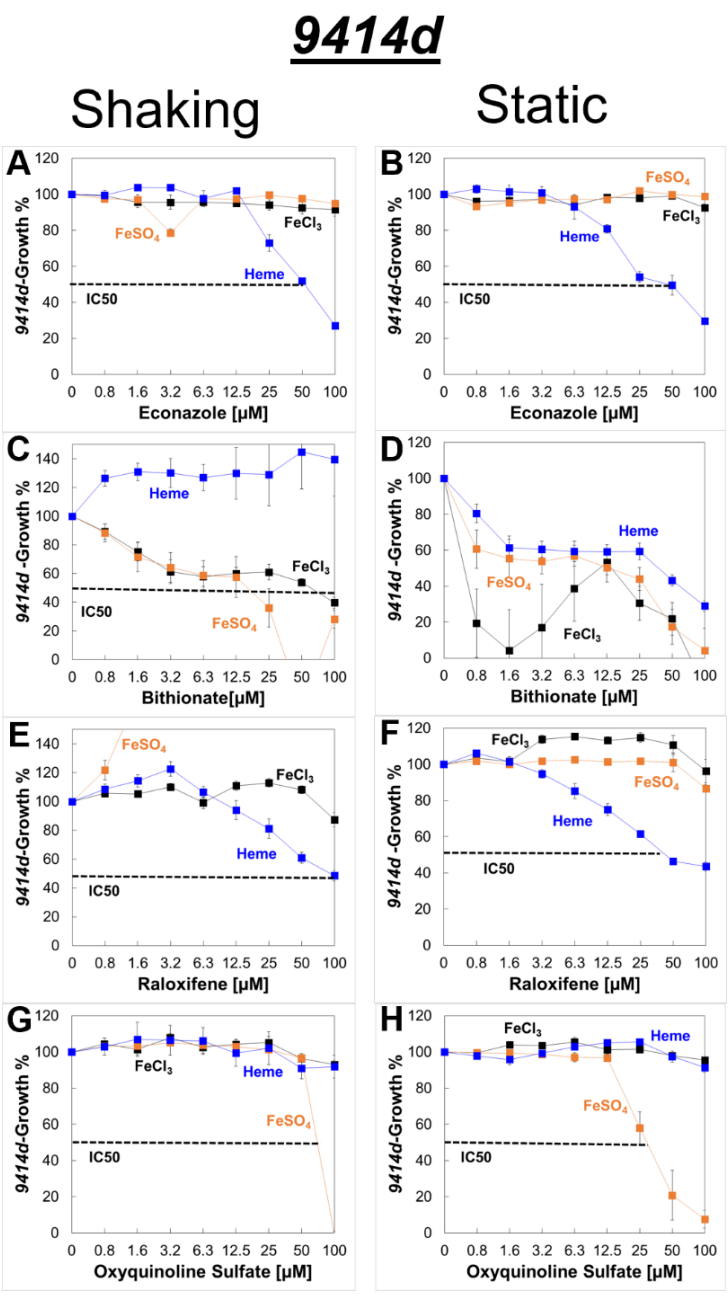

Figure 3.15. *9414d* Shaking and Static growth experiments-
Survival of 9414d in SMM-CAA containing 15 μM $FeCl_3$ (black squares) or 15 μM heme (blue squares) or 15 μM $FeSO_4$ (orange squares) with increasing concentrations of econazole (**A, B)** bithionate (**C, D)** raloxifene **(E, F)** and oxyquinoline sulfate **(G, H).** Growth of the clinical isolate was measured at endpoint OD_{600} at 10 hours with growth percentage determined by relative growth of isolate in the absence of any hit molecules. Error bars represent SEM of five replicates.

3.4 Discussion

In our initial study we demonstrated that a targeted whole-cell HTS can be used to identify iron acquisition inhibitors of *Pa*, but there were questions left unanswered as to how these molecules are inhibiting iron acquisition of *Pa*. Our initial hypothesis was that our hit molecules could be binding the iron source to prevent iron availability, or the molecules could be blocking some cell surface receptor/transporter protein to prevent uptake of the specific iron source.

If the molecules are binding a cell surface protein, then we hypothesized that increasing the *Pa* cell density in dose-response assays this would increase the abundance of cell surface receptor/transporter allowing *Pa* to overcome the inhibitory activity of the hit molecules. For this hypothesis, we tested our best hit molecules the HSIs, econazole and bithionate, and the FSI oxyquinoline sulfate. Increasing the inoculum only modestly affected antipseudomonal activity of econazole in heme (Fig. 3.1). Since increasing cell surface protein abundance through higher cell inoculum does not overcome the inhibitory activity of econazole, this suggests that econazole could be sequestering the heme molecule through binding thus reducing heme availability. There is precedence for this hypothesis because azole molecules like econazole are known to bind heme. In contrast to econazole, increasing the cell inoculum significantly relieved the inhibitory activity of both bithionate (Fig. 3.2) and oxyquinoline sulfate (Fig. 3.3). These observations suggest that bithionate and oxyquinoline sulfate are likely inhibiting heme acquisition by binding some cell surface protein of *Pa*. Since bithionate is a HSI, it is possible that it binds and block activity of the heme outer membrane receptors PhuR or HasR. Alternatively, it is possible that bithionate also blocks activity of the periplasmic protein PhuT or the PhuUV ABC transporter which is involved in heme acquisition. Ferrous iron is hypothesized to be transported across the outer membrane by a porin and then by the Feo ABC transporter across the inner membrane. It is possible that oxyquinoline sulfate could be blocking any of these components to prevent ferrous iron utilization.

It should be noted that we only predict that increasing cell density also increases abundance of cell surface proteins. The most optimal approach to test our transporter/receptor hypothesis is through direct overexpression of genes that encode the transporter proteins of the specific iron acquisition system. In this experiment, we would use *Pa* cells overexpressing the transporter genes in the dose-response assays with the initial cell inoculum of OD_{600} of 0.01 as done previously. Since increasing cell density did not affect econazole activity (Fig. 3.1), we would expect that overexpression of heme acquisition genes also would not affect econazole inhibitory activity. In contrast, we would expect overexpression of heme acquisition genes would overcome bithionate inhibitory activity because increasing cell density allows *Pa* to overcome bithionate activity (Fig. 3.2). Similarly, if oxyquinoline sulfate blocks the Feo ABC transporter, then we would expect *feo* overexpression to overcome inhibitory activity of oxyquinoline sulfate. If *feo* overexpression has no effect, then it would suggest that oxyquinoline sulfate inhibits some outer membrane transporter that is needed for ferrous iron uptake. This would present us with a unique opportunity to identify this component as this transporter for ferrous iron is currently unknown. Selection of resistant mutants could allow us to identify what outer membrane channel proteins are required for ferrous iron uptake, which would then allow us to develop more specific targeted inhibitor molecules.

We also explored the hypothesis that hit molecules could also be binding the iron source. We first tested whether the HSIs econazole, bithionate and raloxifene bind the heme molecule. Tannic acid and zinc pyrithione, the surprise hits, were also included in this analysis because they inhibit *Pa* growth in both ferric and heme iron. Since, econazole and other azole like drugs are known to bind heme, as a control molecule we expected that econazole would interfere with the heme absorption spectra. However, econazole had no effect on the heme absorption spectra. In fact, none of the molecules tested in this assay had any influence of the heme spectra. This would

suggest that these molecules do not bind heme or that even if they bind heme there is no effect on heme absorption, which highlights a limitation of this assay. An ideal way to determine if any of these molecules bind heme would be through direct binding assays such as isothermal titration calorimetry. It is known that molecules such as tannic acid and oxyquinoline sulfate exhibit iron chelating activity. Thus, we used the Chrome Azurol S (CAS) assay to test whether any of the hit molecules have direct iron chelating activity. As expected only tannic acid and oxyquinoline sulfate displayed iron chelating compared to our control molecule EDTA (Fig. 3.10). It should be noted that the CAS assay specifically tests for ferric iron chelating properties. Since oxyquinoline sulfate shows inhibitory activity in the presence of ferrous iron, we do not know if it could also chelate ferrous iron.

A most exciting observation of this study was that many of the hit molecules identified from our screen also showed activity against multi-drug resistant *Pa* isolates. Since our initial screen was performed using the lab strain *Pa* PAO1 isolate, a drawback was that we did not know if the hit molecules would be active against other isolates. A general unifying finding was that all hit molecules except bithionate were active in clinical *Pa* isolates (Fig. 3.12-3.15), and they displayed iron specific activity. Bithionate did not show any iron specific activity against all the clinical isolates highlighting genetic and molecular differences between the clinical isolates and PAO1 isolate. All other hit molecules were also active against the clinical *Pa* isolates grown statically which supports biofilm formation. In fact, raloxifene displayed increased activity against *Pa* isolates under biofilm growth conditions compared to grown planktonically. These observations are incredibly significant findings as many molecules that inhibit growth of planktonic *Pa* can lose activity against *Pa* in biofilms. A clear limitation of the current hit molecules is that they exhibit micromolar levels of antipseudomonal activity. However, from this

pilot screen we were able to identify structurally diverse molecules that can serve as a platform to rationally design or synthesize more targeted compound libraries for future high throughput screens. Furthermore, the molecules are active against clinical *Pa* isolates demonstrating that they inhibit broadly conserved mechanisms across *Pa* isolates.

CHAPTER IV

CONCLUSION

In this research study we presented a proof of concept of a targeted screening approach that identifies molecules blocking specific iron acquisition systems. We also identified structurally diverse molecules that specifically inhibit *Pa* in the presence of either heme or ferrous iron. Once these molecules were investigated their mechanisms of action and their activity against clinical *Pa* isolates. Initially we investigated the mechanisms of action of the hits by exposing *Pa* to a higher concentration of iron where we did not see an effect on antipseudomonal activity (Fig. 2.5). We then examined if increasing the cell count of WT against these hits would change the antipseudomonal activity. The purpose of this experiment was to increase the cell count theoretically increasing the amount of available transport proteins. Antipseudomonal activity in the presence of econazole remained similar after increasing the inoculum, in bithionate activity shifted but antipseudomonal activity was not abolished (Figs 3.1-3.2). Increasing inoculum recovered growth in the presence of oxyquinoline sulfate **(**Figs. 3.3). With there being no change in activity in econazole, it is possible that econazole is binding heme molecule preventing uptake, this being supported by azole drugs being known to bind heme. Econazole also showed no chelation activity in the CAS experiment (Fig. 3.10). In bithionate when increasing WT cells, we see a slight recovery of the cells however antipseudomonal activity is still present. We also see no chelating activity in bithionate similar to econazole (Fig. 3.11). Previously we identified at 15 µM

bithionate antipseudomonal activity is partially alleviated suggesting possible binding of outer membrane receptors, PhuR and HasR, or heme acquisition periplasmic proteins like PhuT.

In the FSI oxyquinoline sulfate growth recovery was seen with the addition of a higher inoculum confirming what we had proposed that oxyquinoline sulfate binding to a portion of the cell due to the growth recovery we see in the increased inoculum experiments (Fig. 3.3). We also saw slight binding activity in the CAS assay confirming oxyquinoline sulfate is known to bind different metals (Fig. 3.10).

In the absorbance experiments all of the HSIs as well as our surprise hits showed inconclusive results. There were no predictable shifts in absorbance and thus no way to conclude if there is possible binding activity. Binding could occur with no change to the original absorbance values. As mentioned previously direct binding assays such as isothermal titration calorimetry would be a better way to determine if binding is occurring with our hits and heme.

When examining the chelation activity of our surprise hits strong chelating activity occurred with tannic acid while no chelation activity was seen in ZPT (Fig. 3.10). Although tannic acid shows chelation activity, possibly explaining the antipseudomonal activity in ferric conditions, the mechanism is still unclear for these surprise hits. Previously we proposed these hits may be targeting a common component in the ferric and heme pathways, the TonB-ExbBD proteins. This could be examined by creating a deletion mutant of *tonB* as seen in Takase *et al.* In their assay growth of the *tonB* mutant did not occur in an iron free minimal media without excess ferrous iron[106]. By taking a *tonB* mutant and growing in minimal media supplemented with ferrous iron, then introducing either surprise hit we can examine if the surprise hits are targeting

the TonB-ExbBD system. Any decline in growth in the *tonB* mutant in the presence of the surprise hits would suggest another mechanism of action other than TonB-ExbBD.

Excitingly we also examined our HSIs and FSI against clinical isolates where we saw activity in the majority of the isolates tested. Unfortunately, the first isolate *5715d* did not show any specific activity across any of the hits (Fig. 3.12) whereas *112014b, 3614b* and *9414d* had significant specific activity in econazole, raloxifene, and oxyquinoline sulfate in their respective iron source (Fig.3.13-3.15). This was not only present in shaking conditions but in static as well, which we used to simulate biofilm forming conditions. We even saw stronger activity in the static conditions than in the shaking conditions with some compounds. This is extremely exciting as one of the major virulence factors of *Pa* is the ability to produce biofilm and become antibiotic resistant and seeing activity of compounds in clinical isolates, some of which activity is greater in static biofilm forming conditions is promising. In the future, examination of both PAO1 and the *Pa* clinical isolates in a more relevant media to that of an infection and our hit compounds. For example, exposing strains to artificial sputum media that mimic the conditions of a CF lung environment then introducing our hit compounds in these conditions to determine if activity is retained.

We understand that this is all very preliminary, some of our compounds like econazole are cytotoxic, and could not be used as chemotherapy. However, we showed proof of concept that this pilot screen identified structurally diverse compounds effective against WT PAO1 and three clinical isolates. We eventually hope to use this screen as a base for eventually larger HTS with larger compound libraries. A larger HTS would allow for more exposure to compounds and identification of newer compounds that may not be FDA approved yet. We hope to one day identify a cocktail of iron inhibitors to block all three iron acquisition pathways simultaneously in *Pa* while

also being effective in other gram-negative pathogens. Some other avenues yet to be explored are PAO1 and the *Pa* clinical isolates in a more infection like environment. Also examining the hits present simultaneously, how our hits interact with other clinically approved antibiotics and finally examining these hits against other gram-negative pathogens. Investigating two hits from the same category such as econazole and raloxifene together would be interesting to see with the assumption that they would work synergistically to target the heme pathways of *Pa*. Initially we examined econazole, bithionate and oxyquinoline sulfate against a beta-lactam antibiotic meropenem which showed no interfering activity with oxyquinoline actually potentiating the activity. In the future all hits should be examined in the presence of meropenem or other clinical antibiotics to test for interfering or potentiating activity. This screening approach can be adapted easily to other pathogens and since the gram-negative iron acquisition pathways are similar between bacterial species these compounds may be effective against other gram-negative pathogens.

REFERENCES

1. Wallace, D.F., *The Regulation of Iron Absorption and Homeostasis.* Clin Biochem Rev, 2016. **37**(2): p. 51-62.
2. Micronutrients., I.o.M.U.P.o., *Dietary Reference Intakes for Vitamin A, Vitamin K, Arsenic, Boron, Chromium, Copper, Iodine, Iron, Manganese, Molybdenum, Nickel, Silicon, Vanadium, and Zinc*. 2001: National Academy Press. 107.
3. Pittman, R.N., in *Regulation of Tissue Oxygenation*. 2011: San Rafael (CA).
4. Beard, J.L., *Iron Biology in Immune Function, Muscle Metabolism and Neuronal Functioning.* The Journal of Nutrition, 2001. **131**(2): p. 568S-580S.
5. Evstatiev, R. and C. Gasche, *Iron sensing and signalling.* Gut, 2012. **61**(6): p. 933-952.
6. Liu, J., et al., *Metalloproteins Containing Cytochrome, Iron–Sulfur, or Copper Redox Centers.* Chemical Reviews, 2014. **114**(8): p. 4366-4469.
7. Puig, S., et al., *The elemental role of iron in DNA synthesis and repair.* Metallomics, 2017. **9**(11): p. 1483-1500.
8. Chifman, J., R. Laubenbacher, and S.V. Torti, *A systems biology approach to iron metabolism*. Adv Exp Med Biol, 2014. **844**: p. 201-25.
9. Caza, M. and J. Kronstad, *Shared and distinct mechanisms of iron acquisition by bacterial and fungal pathogens of humans.* Frontiers in Cellular and Infection Microbiology, 2013. **3**.
10. Brown, J.S. and D.W. Holden, *Iron acquisition by Gram-positive bacterial pathogens.* Microbes and Infection, 2002. **4**(11): p. 1149-1156.
11. Pasqua, M., et al., *Ferric Uptake Regulator Fur Is Conditionally Essential in Pseudomonas aeruginosa.* Journal of Bacteriology, 2017. **199**(22): p. e00472-17.
12. Page, M.G.P., *The Role of Iron and Siderophores in Infection, and the Development of Siderophore Antibiotics.* Clin Infect Dis, 2019. **69**(Supplement_7): p. S529-S537.
13. Harrington, J.M. and A.L. Crumbliss, *The redox hypothesis in siderophore-mediated iron uptake.* BioMetals, 2009. **22**(4): p. 679-689.
14. Cartron, M.L., et al., *Feo--transport of ferrous iron into bacteria.* Biometals, 2006. **19**(2): p. 143-57.
15. Sheldon, J.R. and D.E. Heinrichs, *Recent developments in understanding the iron acquisition strategies of gram positive pathogens.* FEMS Microbiology Reviews, 2015. **39**(4): p. 592-630.
16. Dumas, Z., A. Ross-Gillespie, and R. Kümmerli, *Switching between apparently redundant iron-uptake mechanisms benefits bacteria in changeable environments.* Proc Biol Sci, 2013. **280**(1764): p. 20131055.
17. Bonneau, A., B. Roche, and I.J. Schalk, *Iron acquisition in Pseudomonas aeruginosa by the siderophore pyoverdine: an intricate interacting network including periplasmic and membrane proteins.* Sci Rep, 2020. **10**(1): p. 120.
18. Brillet, K., et al., *An ABC transporter with two periplasmic binding proteins involved in iron acquisition in Pseudomonas aeruginosa.* ACS Chem Biol, 2012. **7**(12): p. 2036-45.

19. Paulen, A., et al., *Synthesis of conjugates between oxazolidinone antibiotics and a pyochelin analogue.* Bioorganic & Medicinal Chemistry Letters, 2017. **27**(21): p. 4867-4870.
20. Cornelis, P. and J. Dingemans, *Pseudomonas aeruginosa adapts its iron uptake strategies in function of the type of infections.* Front Cell Infect Microbiol, 2013. **3**: p. 75.
21. Bhakta, M.N. and A. Wilks, *The mechanism of heme transfer from the cytoplasmic heme binding protein PhuS to the delta-regioselective heme oxygenase of Pseudomonas aeruginosa.* Biochemistry, 2006. **45**(38): p. 11642-9.
22. Poole, K., et al., *Cloning and nucleotide sequence analysis of the ferripyoverdine receptor gene fpvA of Pseudomonas aeruginosa.* J Bacteriol, 1993. **175**(15): p. 4597-604.
23. Ghysels, B., et al., *FpvB, an alternative type I ferripyoverdine receptor of Pseudomonas aeruginosa.* Microbiology, 2004. **150**(Pt 6): p. 1671-1680.
24. Ochsner, U.A., Z. Johnson, and M.L. Vasil, *Genetics and regulation of two distinct haem-uptake systems, phu and has, in Pseudomonas aeruginosa.* Microbiology, 2000. **146 (Pt 1)**: p. 185-198.
25. Smith, A.D., et al., *Spectroscopic Determination of Distinct Heme Ligands in Outer-Membrane Receptors PhuR and HasR of Pseudomonas aeruginosa.* Biochemistry, 2015. **54**(16): p. 2601-12.
26. Ganne, G., et al., *Iron Release from the Siderophore Pyoverdine in Pseudomonas aeruginosa Involves Three New Actors: FpvC, FpvG, and FpvH.* ACS Chem Biol, 2017. **12**(4): p. 1056-1065.
27. Huang, W. and A. Wilks, *Extracellular Heme Uptake and the Challenge of Bacterial Cell Membranes.* Annu Rev Biochem, 2017.
28. Gi, M., et al., *A novel siderophore system is essential for the growth of Pseudomonas aeruginosa in airway mucus.* Sci Rep, 2015. **5**: p. 14644.
29. Weinstein, R.A., et al., *Overview of Nosocomial Infections Caused by Gram-Negative Bacilli.* Clinical Infectious Diseases, 2005. **41**(6): p. 848-854.
30. Klockgether, J., et al., *Long-Term Microevolution of Pseudomonas aeruginosa Differs between Mildly and Severely Affected Cystic Fibrosis Lungs.* Am J Respir Cell Mol Biol, 2018. **59**(2): p. 246-256.
31. Bhagirath, A.Y., et al., *Cystic fibrosis lung environment and Pseudomonas aeruginosa infection.* BMC Pulm Med, 2016. **16**(1): p. 174.
32. Minandri, F., et al., *Role of Iron Uptake Systems in Pseudomonas aeruginosa Virulence and Airway Infection.* Infect Immun, 2016. **84**(8): p. 2324-2335.
33. Kang, D., et al., *Pyoverdine-Dependent Virulence of Pseudomonas aeruginosa Isolates From Cystic Fibrosis Patients.* Front Microbiol, 2019. **10**: p. 2048.
34. Konings, A.F., et al., *Pseudomonas aeruginosa uses multiple pathways to acquire iron during chronic infection in cystic fibrosis lungs.* Infect Immun, 2013. **81**(8): p. 2697-704.
35. De Vos, D., et al., *Study of pyoverdine type and production by Pseudomonas aeruginosa isolated from cystic fibrosis patients: prevalence of type II pyoverdine isolates and accumulation of pyoverdine-negative mutations.* Arch Microbiol, 2001. **175**(5): p. 384-8.
36. Nguyen, A.T., et al., *Adaptation of iron homeostasis pathways by a Pseudomonas aeruginosa pyoverdine mutant in the cystic fibrosis lung.* J Bacteriol, 2014. **196**(12): p. 2265-76.

37. Hunter, R.C., et al., *Ferrous iron is a significant component of bioavailable iron in cystic fibrosis airways.* mBio, 2013. **4**(4).
38. Reinhart, A.A. and A.G. Oglesby-Sherrouse, *Regulation of Pseudomonas aeruginosa Virulence by Distinct Iron Sources.* Genes (Basel), 2016. **7**(12).
39. Bjorn, M.J., et al., *Effect of iron on yields of exotoxin A in cultures of Pseudomonas aeruginosa PA-103.* Infect Immun, 1978. **19**(3): p. 785-91.
40. Vasil, M.L., et al., *The fur-regulated gene encoding the alternative sigma factor PvdS is required for iron-dependent expression of the LysR-type regulator ptxR in Pseudomonas aeruginosa.* J Bacteriol, 1998. **180**(24): p. 6784-8.
41. Gaines, J.M., et al., *Regulation of the Pseudomonas aeruginosa toxA, regA and ptxR genes by the iron-starvation sigma factor PvdS under reduced levels of oxygen.* Microbiology, 2007. **153**(12): p. 4219-4233.
42. Wang, Y., et al., *Phenazine-1-carboxylic acid promotes bacterial biofilm development via ferrous iron acquisition.* J Bacteriol, 2011. **193**(14): p. 3606-17.
43. Ochsner, U.A., et al., *GeneChip expression analysis of the iron starvation response in Pseudomonas aeruginosa: identification of novel pyoverdine biosynthesis genes.* Mol Microbiol, 2002. **45**(5): p. 1277-87.
44. Banin, E., M.L. Vasil, and E.P. Greenberg, *Iron and Pseudomonas aeruginosa biofilm formation.* Proc Natl Acad Sci U S A, 2005. **102**(31): p. 11076-81.
45. Berlutti, F., et al., *Iron Availability Influences Aggregation, Biofilm, Adhesion and Invasion of Pseudomonas Aeruginosa and Burkholderia Cenocepacia.* International Journal of Immunopathology and Pharmacology, 2005. **18**(4): p. 661-670.
46. Mouriño, S., et al., *Metabolite-driven Regulation of Heme Uptake by the Biliverdin IXβ/δ-Selective Heme Oxygenase (HemO) of Pseudomonas aeruginosa.* J Biol Chem, 2016. **291**(39): p. 20503-15.
47. Goss, C.H., et al., *Gallium disrupts bacterial iron metabolism and has therapeutic effects in mice and humans with lung infections.* Sci Transl Med, 2018. **10**(460).
48. Kang, D., et al., *Pyoverdine Inhibitors and Gallium Nitrate Synergistically Affect Pseudomonas aeruginosa.* mSphere, 2021. **6**(3): p. e00401-21.
49. Kirienko, D.R., D. Kang, and N.V. Kirienko, *Novel Pyoverdine Inhibitors Mitigate Pseudomonas aeruginosa Pathogenesis.* Front Microbiol, 2018. **9**: p. 3317.
50. Silby, M.W., et al., *Pseudomonas genomes: diverse and adaptable.* FEMS Microbiol Rev, 2011. **35**(4): p. 652-80.
51. Gaynes, R., J.R. Edwards, and S. National Nosocomial Infections Surveillance, *Overview of nosocomial infections caused by gram-negative bacilli.* Clin Infect Dis, 2005. **41**(6): p. 848-54.
52. Weiner-Lastinger, L.M., et al., *Antimicrobial-resistant pathogens associated with adult healthcare-associated infections: Summary of data reported to the National Healthcare Safety Network, 2015-2017.* Infect Control Hosp Epidemiol, 2020. **41**(1): p. 1-18.
53. Magill, S.S., et al., *Multistate point-prevalence survey of health care-associated infections.* N Engl J Med, 2014. **370**(13): p. 1198-208.
54. Blanchette, C.M., et al., *Healthcare Cost and Utilization before and after Diagnosis of Pseudomonas aeruginosa among Patients with Non-Cystic Fibrosis Bronchiectasis in the U.S.* Med Sci (Basel), 2017. **5**(4).

55. Cabot, G., et al., *Pseudomonas aeruginosa ceftolozane-tazobactam resistance development requires multiple mutations leading to overexpression and structural modification of AmpC.* Antimicrob Agents Chemother, 2014. **58**(6): p. 3091-9.
56. Tacconelli, E., N. Magrini, and W.H. Organization, *Global priority list of antibiotic-resistant bacteria to guide research, discovery, and development of new antibiotics.* http://www.who.int/medicines/publications/globalpriority-list-antibiotic-resistant-bacteria/en/. 2017.
57. Skaar, E.P., *The battle for iron between bacterial pathogens and their vertebrate hosts.* PLoS Pathog, 2010. **6**(8): p. e1000949.
58. Hood, M.I. and E.P. Skaar, *Nutritional immunity: transition metals at the pathogen-host interface.* Nat Rev Microbiol, 2012. **10**(8): p. 525-37.
59. Cox, C.D., *Effect of pyochelin on the virulence of Pseudomonas aeruginosa.* Infect Immun, 1982. **36**(1): p. 17-23.
60. Kirienko, N.V., et al., *Pseudomonas aeruginosa disrupts Caenorhabditis elegans iron homeostasis, causing a hypoxic response and death.* Cell Host Microbe, 2013. **13**(4): p. 406-16.
61. Takase, H., et al., *Impact of siderophore production on Pseudomonas aeruginosa infections in immunosuppressed mice.* Infect Immun, 2000. **68**(4): p. 1834-9.
62. Meyer, J.M., et al., *Pyoverdin is essential for virulence of Pseudomonas aeruginosa.* Infect Immun, 1996. **64**(2): p. 518-23.
63. Smith, D.J., et al., *Targeting iron uptake to control Pseudomonas aeruginosa infections in cystic fibrosis.* Eur Respir J, 2013. **42**(6): p. 1723-36.
64. Runyen-Janecky, L.J., *Role and regulation of heme iron acquisition in gram-negative pathogens.* Front Cell Infect Microbiol, 2013. **3**: p. 55.
65. Meyer, J.M. and M.A. Abdallah, *The fluorescent pigment of Pseudomonas fluorescens: Biosynthesis, purification and physicochemical properties.* Microbiology, 1978. **107**(2): p. 319-328.
66. Palmer, K.L., L.M. Aye, and M. Whiteley, *Nutritional cues control Pseudomonas aeruginosa multicellular behavior in cystic fibrosis sputum*. J Bacteriol, 2007. **189**(22): p. 8079-87.
67. Ghani, M. and J.S. Soothill, *Ceftazidime, gentamicin, and rifampicin, in combination, kill biofilms of mucoid Pseudomonas aeruginosa.* Can J Microbiol, 1997. **43**(11): p. 999-1004.
68. Sriramulu, D.D., et al., *Microcolony formation: a novel biofilm model of Pseudomonas aeruginosa for the cystic fibrosis lung.* J Med Microbiol, 2005. **54**(Pt 7): p. 667-676.
69. Fung, C., et al., *Gene expression of Pseudomonas aeruginosa in a mucin-containing synthetic growth medium mimicking cystic fibrosis lung sputum*. J Med Microbiol, 2010. **59**(Pt 9): p. 1089-1100.
70. Hare, N.J., et al., *Proteomics of Pseudomonas aeruginosa Australian epidemic strain 1 (AES-1) cultured under conditions mimicking the cystic fibrosis lung reveals increased iron acquisition via the siderophore pyochelin.* J Proteome Res, 2012. **11**(2): p. 776-95.
71. Kirchner, S., et al., *Use of artificial sputum medium to test antibiotic efficacy against Pseudomonas aeruginosa in conditions more relevant to the cystic fibrosis lung.* J Vis Exp, 2012(64): p. e3857.
72. Quinn, R.A., et al., *A Winogradsky-based culture system shows an association between microbial fermentation and cystic fibrosis exacerbation.* ISME J, 2015. **9**(4): p. 1052.

73. Turner, K.H., et al., *Essential genome of Pseudomonas aeruginosa in cystic fibrosis sputum*. Proc Natl Acad Sci U S A, 2015. **112**(13): p. 4110-5.
74. Iversen, P.W., et al., *HTS Assay Validation*, in *Assay Guidance Manual*, S. Markossian, et al., Editors. 2004: Bethesda (MD).
75. Cornelis, P., *Iron uptake and metabolism in pseudomonads.* Appl Microbiol Biotechnol, 2010. **86**(6): p. 1637-45.
76. Crichton, R.R. and J.L. Pierre, *Old iron, young copper: from Mars to Venus.* Biometals, 2001. **14**(2): p. 99-112.
77. Balding, P.R., et al., *How do azoles inhibit cytochrome P450 enzymes? A density functional study.* J Phys Chem A, 2008. **112**(50): p. 12911-8.
78. Greule, A., et al., *Unrivalled diversity: the many roles and reactions of bacterial cytochromes P450 in secondary metabolism*. Nat Prod Rep, 2018. **35**(8): p. 757-791.
79. Nelson, D.R., *The cytochrome p450 homepage.* Hum Genomics, 2009. **4**(1): p. 59-65.
80. Tooker, B.C., et al., *Pseudomonas aeruginosa cytochrome P450 CYP168A1 is a fatty acid hydroxylase that metabolizes arachidonic acid to the vasodilator 19-HETE*. J Biol Chem, 2022. **298**(3): p. 101629.
81. Ho Sui, S.J., et al., *Raloxifene attenuates Pseudomonas aeruginosa pyocyanin production and virulence.* Int J Antimicrob Agents, 2012. **40**(3): p. 246-51.
82. Zhao, L., et al., *Determination of cadmium(II), cobalt(II), nickel(II), lead(II), zinc(II), and copper(II) in water samples using dual-cloud point extraction and inductively coupled plasma emission spectrometry.* J Hazard Mater, 2012. **239-240**: p. 206-12.
83. Henry, C., et al., *New 8-hydroxyquinoline and catecholate iron chelators: influence of their partition coefficient on their biological activity.* Biochem Pharmacol, 2001. **62**(10): p. 1355-62.
84. Chupakhina, T.A., A.M. Katsev, and V.O. Kur'ianov, *[Synthesis and antimicrobial ivestigation of 8-quinolinols glucosaminides]*. Bioorg Khim, 2012. **38**(4): p. 482-8.
85. du Moulinet d'Hardemare, A., et al., *Oxinobactin and sulfoxinobactin, abiotic siderophore analogues to enterobactin involving 8-hydroxyquinoline subunits: thermodynamic and structural studies.* Inorg Chem, 2012. **51**(22): p. 12142-51.
86. Greenberg, J., S.S. Turesky, and V.D. Warner, *Effects of metal salts in prolonging antibacterial activity of teeth treated with 8-hydroxyquinoline.* J Periodontol, 1976. **47**(11): p. 664-6.
87. He, W., et al., *Evaluation of the anti-biofilm activities of bacterial cellulose-tannic acid-magnesium chloride composites using an in vitro multispecies biofilm model.* Regen Biomater, 2021. **8**(6): p. rbab054.
88. Abdel Malek, S.M., et al., *Pseudomonas aeruginosa PAO1 resistance to Zinc pyrithione: phenotypic changes suggest the involvement of efflux pumps.* Curr Microbiol, 2009. **59**(2): p. 95-100.
89. Fu, Z. and R. Chen, *Study of Complexes of Tannic Acid with Fe(III) and Fe(II).* J Anal Methods Chem, 2019. **2019**: p. 3894571.
90. Guthery, E., L.A. Seal, and E.L. Anderson, *Zinc pyrithione in alcohol-based products for skin antisepsis: persistence of antimicrobial effects.* Am J Infect Control, 2005. **33**(1): p. 15-22.
91. Reeder, N.L., et al., *Zinc pyrithione inhibits yeast growth through copper influx and inactivation of iron-sulfur proteins.* Antimicrob Agents Chemother, 2011. **55**(12): p. 5753-60.

92. Rouault, T.A. and W.H. Tong, *Tangled up in red: intertwining of the heme and iron-sulfur cluster biogenesis pathways.* Cell Metab, 2009. **10**(2): p. 80-1.
93. Park, M., et al., *Understanding the Mechanism of Action of the Anti-Dandruff Agent Zinc Pyrithione against Malassezia restricta.* Sci Rep, 2018. **8**(1): p. 12086.
94. Wilson, B.R., et al., *Siderophores in Iron Metabolism: From Mechanism to Therapy Potential.* Trends Mol Med, 2016. **22**(12): p. 1077-1090.
95. Caza, M. and J.W. Kronstad, *Shared and distinct mechanisms of iron acquisition by bacterial and fungal pathogens of humans.* Front Cell Infect Microbiol, 2013. **3**: p. 80.
96. Richard, K.L., B.R. Kelley, and J.G. Johnson, *Heme Uptake and Utilization by Gram-Negative Bacterial Pathogens.* Front Cell Infect Microbiol, 2019. **9**: p. 81.
97. Santajit, S. and N. Indrawattana, *Mechanisms of Antimicrobial Resistance in ESKAPE Pathogens.* Biomed Res Int, 2016. **2016**: p. 2475067.
98. Marturano, J.E. and T.J. Lowery, *ESKAPE Pathogens in Bloodstream Infections Are Associated With Higher Cost and Mortality but Can Be Predicted Using Diagnoses Upon Admission.* Open Forum Infect Dis, 2019. **6**(12): p. ofz503.
99. Heel, R.C., et al., *Econazole: a review of its antifungal activity and therapeutic efficacy.* Drugs, 1978. **16**(3): p. 177-201.
100. Bennett, J.E., R. Dolin, and M.J. Blaser, *Preface to the Eighth Edition*, in *Mandell, Douglas, and Bennett's Principles and Practice of Infectious Diseases (Eighth Edition)*, J.E. Bennett, R. Dolin, and M.J. Blaser, Editors. 2015, W.B. Saunders: Philadelphia. p. xxvii.
101. Quintanilla Rodriguez BS, C.R. *Raloxifene* 2022 [cited 2023; Available from: https://www.ncbi.nlm.nih.gov/books/NBK544233/?report=reader.
102. Information, N.C.f.B., PubChem, 2023(Oxyquinoline Sulfate).
103. Kaczmarek, B., *Tannic Acid with Antiviral and Antibacterial Activity as A Promising Component of Biomaterials-A Minireview*. Materials (Basel), 2020. **13**(14).
104. Schwartz, J.R., *Zinc Pyrithione: A Topical Antimicrobial With Complex Pharmaceutics.* J Drugs Dermatol, 2016. **15**(2): p. 140-4.
105. Kannon, M., et al., *A Novel Approach To Identify Inhibitors of Iron Acquisition Systems of Pseudomonas aeruginosa.* Microbiology Spectrum. **0**(0): p. e02437-22.
106. Takase, H., et al., *Requirement of the Pseudomonas aeruginosa tonB gene for high-affinity iron acquisition and infection.* Infect Immun, 2000. **68**(8): p. 4498-504.

VITA

Mamie Kannon

Candidate for the Degree of

Master of Science

Thesis: BLOCKING THE ACQUISITION OF THE ESSENTIAL IRON NUTRIENT IN *PSEUDOMONAS AERUGINOSA*

Major Field: Microbiology, Cell and Molecular Biology

Biographical:

Education:

Completed the requirements for the Master of Science in Microbiology, Cell and Molecular Biology at Oklahoma State University, Stillwater, Oklahoma in May, 2023.

Completed the requirements for the Bachelor of Science in Microbiology, Cell and Molecular Biology at Oklahoma State University, Stillwater, Oklahoma in 2020.

Experience:

Performance of molecular biology laboratory techniques.

Mentor for undergraduate researchers

Teaching assistant for undergraduate courses

Publications:

Kannon, M., et al., A Novel Approach to Identify Inhibitors of Iron Acquisition Systems of Pseudomonas aeruginosa. Microbiology Spectrum. 0 (0): p. e02437-22.